FINAL REPORT

TRANSPORT PHENOMENA IN THIN ROTATING LIQUID FILMS INCLUDING NUCLEATE BOILING

NASA Grant No. NCC3-789

PI: Amir Faghri
Co-PI: Baki M. Cetegen

Executive Summary

In this grant, experimental, numerical and analytical studies of heat transfer in a thin liquid film flowing over a rotating disk have been conducted. Heat transfer coefficients were measured experimentally in a rotating disk heat transfer apparatus where the disk was heated from below with electrical resistance heaters. The heat transfer measurements were supplemented by experimental characterization of the liquid film thickness using a novel laser based technique. The heat transfer measurements show that the disk rotation plays an important role on enhancement of heat transfer primarily through the thinning of the liquid film. Experiments covered both momentum and rotation dominated regimes of the flow and heat transfer in this apparatus. Heat transfer measurements have been extended to include evaporation and nucleate boiling and these experiments are continuing in our laboratory. Empirical correlations have also been developed to provide useful information for design of compact high efficiency heat transfer devices. The experimental work has been supplemented by numerical and analytical analyses of the same problem. Both numerical and analytical results have been found to agree reasonably well with the experimental results on liquid film thickness and heat transfer coefficients/Nusselt numbers. The numerical simulations include the free surface liquid film flow and heat transfer under disk rotation including the conjugate effects. The analytical analysis utilizes an integral boundary layer approach from which semi-analytical and/or analytical expressions for the Nusselt number were obtained.

From this research following articles have come out in chronological order:

Ozar, B., Faghri A. and Cetegen, B. M., "Experiments on the flow of a thin liquid film over a horizontal stationary and rotating disk surface," ***Experiments in Fluids***, Vol. 34, pp. 556-565, 2003 (see attached)

Ozar, B., Cetegen, B. M. and Faghri, A., "Experiments on heat transfer in a thin liquid film flowing over a rotating disk," ***ASME Journal of Heat Transfer***, Vol. 126, pp. 184 - 192, April 2004 (see attached)

Rice, J., Faghri, A., Cetegen, B. M., "Analysis of a free surface film from a controlled liquid impingement jet over a rotating disk including conjugate effects with and without evaporation", submitted to ***International Journal of Heat and Mass Transfer***, December 2004 (also to be presented at ASME Summer Heat Transfer Conference, San Francisco, CA, July 17-22, 2005) (see attached)

Basu, S. and Cetegen, B. M., "Analysis of hydrodynamics and heat transfer in a thin liquid film flowing over a rotating disk by integral method," submitted to ***ASME J. Heat Transfer***, April 2005 (see attached)

Proceeding of HT 2005
ASME Summer Heat Transfer Conference
July 17-22, 2005, San Francisco, CA, USA

HT2005-72103

Analysis of a Free Surface Film from a Controlled Liquid Impinging Jet over a Rotating Disk Including Conjugate Effects, with and without Evaporation

Jeremy Rice Amir Faghri Baki M. Cetegen

Department of Mechanical Engineering, University of Connecticut, Storrs, CT 06269-3139

Abstract

A detailed analysis of the liquid film characteristics and the accompanying heat transfer of a free surface controlled liquid impinging jet onto a rotating disk are presented. The computations were run on a two-dimensional axi-symmetric Eulerian mesh while the free surface was calculated with the volume of fluid method. Flow rates between 3 and 15 lpm with rotational speeds between 50 and 200 rpm are analyzed. The effects of inlet temperature on the film thickness and heat transfer are characterized as well as evaporative effects. The conjugate heating effect is modeled, and was found to effect the heat transfer results the most at both the inner and outer edges of the heated surface. The heat transfer was enhanced with both increasing flow rate and increasing rotational speeds. When evaporative effects were modeled, the evaporation was found to increase the heat transfer at the lower flow rates the most because of a fully developed thermal field that was achieved. The evaporative effects did not significantly enhance the heat transfer at the higher flow rates.

1 Introduction

Impinging jets on rotating surfaces have received a lot of attention lately because of the high potential of heat transfer rates that can be achieved. There are two major classes of impinging jets useful for engineering applications; they are the submerged jet and the free jet. A submerged jet is one that flows into a stagnant fluid of similar properties, whereas a free jet is a liquid that flows from a nozzle into a gaseous region, and is virtually unaffected by gas, hence the term free. There are numerous applications of impinging jets, which include material processing, turbine blade cooling and cooling of electronics. In the present study, a controlled liquid impinging jet is studied. A controlled liquid impinging jet flows onto a planar disk; near the center of the disk there is another smaller coaxial disk (collar), which controls the entrance free film thickness and entrance radius of the free film. The present study is motivated because of the envisioned potential of rotating thin film fluids in an absorber unit for a spacecraft vapor-absorption heat pump system. This unit will work in a micro-gravity environment, where the disk can be rotated to apply an additional force to thin the fluid and enhance the heat transfer.

Watson [1] first studied a free liquid jet impinging normally to a planar surface. He assumed that a substantial portion of the flow near the stagnation point was inviscid and was not affected by the planar surface. He used a similarity solution with a boundary layer approximation to determine the film thickness. Chaudhury [2] studied the heat transfer to Watson's analysis in a similar manner. Craik et al. [3] studied the hydraulic jump formed by an impinging jet of liquid onto a planar surface. They took film thickness measurements with a light absorption technique and also did flow visualization. They found a presence of an eddy just downstream of the hydraulic jump. Tong [4] numerically studied a planar liquid jet impinging obliquely to a planar surface. He used the volume of fluid method to track the free surface. The study focused on heat transfer near the stagnation region, and where the maximum heat transfer occurs.

Rahman et al. [5] developed a finite difference solution using boundary-fitted curvilinear coordinates to locate the free surface. In this technique the free surface conformed to one of the computational boundaries. They studied a falling film down a vertical wall; they also studied plane and radial film flows with and without gravity. Faghri et al. [6] later used this numerical technique to model heat transfer from a controlled impinging jet onto a stationary disk with the conjugate heating effects included. The numerical data were compared to the experimental data, and if the conjugate heating effects were not included, an error as large as 100 percent was seen. Thomas et al. [7] experimentally studied the film thickness of a controlled impinging jet on a stationary and rotating disk. The film thickness measurements were taken using a capacitance technique. The research found that the film thickness on the rotating disk was affected by the inertial and frictional forces on the fluid near the center of the disk, and centrifugal forces near the outer edge of the disk. Also the hydraulic jump was found to "wash off" the disk in the presence of a rotational field. Thomas et al. [8] performed a one-dimensional analysis of the hydrodynamic and thermal characteristics of thin film flows with and without rotation with the MacCormack predictor-corrector method. The hydraulic jump was not present in the absence of gravitational forces. However, when the disk was rotated the film thickness was

unaffected by gravitational forces. The heat transfer was found to be much greater with rotation because the liquid film is much thinner and is moving with a higher velocity.

Rahman and Faghri [9] solved a three dimensional slice of the flow over a rotating disk using boundary-fitted coordinates; also they improved on Thomas et al.'s [8] model by better approximating the frictional resistance in the azimuthal direction exerted by the solid wall on the flow. They ran cases with heating as well as with evaporation and found that increased flow rate and rotational speed both increased the rate of heat transfer. Most recently, Ozar et al. [10] experimentally studied the heat transfer effects of a thin liquid film from a controlled impinging jet on both a stationary and rotating disk. The fluid mechanics and the heat transfer characteristics were examined simultaneously. Semi-empirical correlations were found to characterize both the local Nusselt number and the average Nusselt number.

From the above literature review, previous numerical models solving liquid jet impingement on a rotating disk mainly involve trial and error methods, which require guessing at the free surface location in some systematic incremental sequence. In the present study, the volume of fluid method is used to track the free surface. This technique requires a single domain, time-dependent solution, which directly locates the free surface once a steady-state solution is achieved, resulting in a highly accurate computation. Furthermore, the free surface has surface tension effects included, which have not previously been modeled properly. The present analysis also includes a conjugate heating effect in the disk, which is sparse in the previous computational work as a single domain problem, and helps to draw better correlations with existing experimental data. Effects of inlet temperatures and flow conditions are studied, which affect both the flow and thermal characteristics of the system. The present analysis also include evaporative cases, or purely heating cases when evaporation is considered negligible. Whether evaporation is important or not is determined by the inlet temperature of the fluid.

Nomenclature

A: Heater area $\pi(r_{hout}^2-r_{hin}^2)$ (m^2)
c: Discharge coefficient for impinging jets
C: Specific heat (joules/kg-K)
d_d: Disk thickness (m)
F: Body force due to surface tension (N/m^3)
g: Gravity (m/s^2)
h: Enthalpy (joules/kg)
k: Thermal conductivity (W/m-k)
$\dot{m}$: Mass flow rate (kg/s)
$\vec{n}$: Normal unit vector
Nu: Local Nusselt number at the disk/liquid interface $\left(\frac{q''r_{in}}{\Delta T \cdot k_l}\right)$
$\overline{Nu}$: Average Nusselt number $\left(\frac{1}{A}\int_A Nu\, dA\right)$
p: Pressure (Pa)
q'': Heat flux, Q/A, (W/m^2)
Q: Heater power, (W)
r: Radial coordinate (m)
r_t: Laminar-turbulent transition radius (m)
r_t^*: Dimensionless laminar-turbulent transition radius $\frac{r_t}{\mathrm{Re}^{*1/3}\sqrt{c2r_{hin}\delta_{in}}}$
Re: Reynolds number $\left(\frac{\dot{m}}{\mu 2\pi r_{hin}}\right)$
Re*: Reynolds number used by Azuma and Hoshino (1984) $\left(\frac{\dot{m}}{\mu\sqrt{c2r_{hin}\delta_{in}}}\right)$
t: Time (s)
$\vec{t}$: Tangential unit vector
T: Temperature (K)
ΔT: Temperature difference, T_w-T_{in} (K)
u: Axial velocity (m/s)
v: Radial velocity (m/s)
$\vec{V}$: Velocity vector (m/s)
$\dot{V}$: Volumetric flow rate (lpm)
w: Swirl velocity (m/s)
x: Axial coordinate (m)

Greek Symbols:

α: Volume fraction of liquid
δ: Film thickness (m)
ϕ: General volume weighted fluid property
κ: Total curvature (m^{-1})
μ: Dynamic viscosity (kg/m-s)
ρ: Density (kg/m^3)
σ: Surface tension (N/m)
ω: Angular velocity (rad/s)

Subscripts:

hin: Inner radius of heater
hout: Outer radius of heater
i: Counting index
in: Inlet
l: Liquid
ref: Reference
t: Laminar-turbulent transition
v: Vapor
w: Disk surface

2 Analysis

Figure 1 shows a schematic of the system being modeled. Flow enters the disk between two circular plates, one being the collar, and the other being the disk. The spacing between the collar and the disk is δ_{in}. After the flow leaves the entrance region between the collar and the disk at r_{hin}, the flow turns from an internal fully developed flow to a free surface flow. The heater provides a constant heat flux at this point, from the bottom of the aluminum disk. The heat is conducted

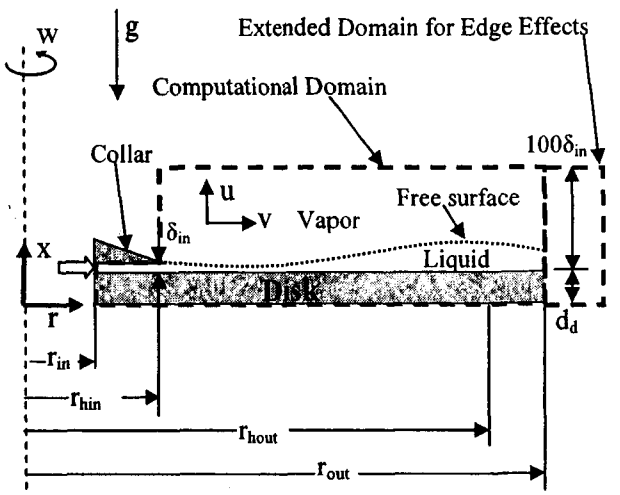

through the disk to the fluid. The basic assumptions of the problem at hand are that the flow field is incompressible, the fluid is considered to be in the laminar flow regime while all of the fluid properties are constant. When evaporation is being modeled, no mass transfer is modeled and the effects are only considered in the energy equation, because the evaporation rate of the liquid is much less than the inlet mass flow rate of the liquid. The Navier-Stokes equations are solved to compute the fluid flow. The continuity, and momentum equations are as follows:

$$\nabla \cdot \vec{V} = 0 \tag{1}$$

$$\rho \frac{D\vec{V}}{Dt} = -\nabla p + \nabla \cdot \left(\mu \nabla \vec{V}\right) + \rho g + F \quad , \tag{2}$$

Since the flow field is assumed to be independent of the temperature field, a steady-state energy equation is solved in the fluid region, once the flow field has been resolved.

$$\nabla \cdot \left(\vec{V} \rho h\right) = \nabla \cdot \left(k \nabla T\right) \tag{4}$$

In the solid region, only conduction is solved.

$$\nabla^2 T = 0 \tag{5}$$

The free surface is tracked by the Volume of Fluid (VOF) method developed by Hirt and Nichols [11], where the volume fraction, α, of the fluid is tracked through each computational cell. The VOF equation is:

$$\frac{\partial \alpha}{\partial t} + \vec{V} \cdot \nabla \alpha = 0 \,. \tag{6}$$

The interface between fluids is represented by a piecewise linear approach, similar to the work of Youngs [12], to greatly limit numerical diffusion of the interface. Surface tension effects are modeled in the present numerical simulations. The surface tension forces are represented by the "F" term in Equation 2. A continuum surface force method proposed by Brackbill [13] is used to model surface tension.

$$F = \sigma \frac{\rho \kappa \nabla \alpha}{0.5\left(\rho_l + \rho_v\right)} \tag{7}$$

The curvature, κ, is defined as:

$$\kappa = \frac{\nabla^2 \alpha}{|\nabla \alpha|} \tag{8}$$

The fluid properties are calculated by the volume weighted average.

$$\phi = \alpha \phi_l + (1 - \alpha) \phi_v \tag{9}$$

The general fluid property, ϕ, represents density, viscosity and thermal conductivity. The enthalpy is calculated using a mass-weighted average, instead of a volume-weighted average.

$$h = \frac{\left[\alpha \rho_l C_l + (1 - \alpha) \rho_v C_v\right]\left(T - T_{ref}\right)}{\rho} \tag{10}$$

The boundary conditions are as follows:

At the inlet $\left(r = r_{in}\right)$

$$\left(0 < x < \delta_{in}\right): \; v = v_{in}, \; T = T_{in} \tag{11-a}$$

$$\left(-d_d < x < 0\right): \; \frac{\partial T}{\partial r} = 0 \tag{11-b}$$

At the collar $\left(x = \delta_{in}, r_{in} < r < r_{hin}\right)$

$$u = v = 0, \; w = \omega r, \; \frac{\partial T}{\partial x} = 0 \tag{12}$$

At the disk surface $\left(x = 0, r_{in} < r < r_{out}\right)$

$$u = v = 0, \; w = \omega r, \; k \frac{\partial T}{\partial x}\bigg|_l = k \frac{\partial T}{\partial x}\bigg|_s \tag{13}$$

At the disk bottom $\left(x = -d_d\right)$

$$\left(r_{in} < r < r_{hin}\right): \qquad k \frac{\partial T}{\partial x}\bigg|_s = 0 \tag{14-a}$$

$$\left(r_{hin} < r < r_{hout}\right): \qquad k \frac{\partial T}{\partial x}\bigg|_s = q'' \tag{14-b}$$

$$\left(r_{hout} < r < r_{out}\right): \qquad k\left.\frac{\partial T}{\partial x}\right|_s = 0 \qquad (14\text{-b})$$

The above variation in heat flux is used to simulate the experimental prediction of Ozar et al. [10].

At the outer boundaries

$\left(r = r_{hin}, \delta_{in} < x < 100\delta_{in}\right), \left(r_{hin} < r < r_{out}, x = 100\delta_{in}\right),$
$\left(r = r_{out}, \delta_{in} < x < 100\delta_{in}\right)$

$$p = p_{ref} \qquad (15\text{-a})$$

$$if\ \left(\vec{V}\cdot\vec{n} > 0\right)\ \frac{\partial T}{\partial \vec{n}} = 0\ else\ T = T_{ref} \qquad (15\text{-b})$$

At the liquid-vapor interface

$$p_l - p_v - \mu_l\left.\frac{\partial \vec{V}\cdot\vec{n}}{\partial \vec{n}}\right|_l + \mu_v\left.\frac{\partial \vec{V}\cdot\vec{n}}{\partial \vec{n}}\right|_v = \sigma\kappa \qquad (16\text{-a})$$

$$\mu_l\left.\frac{\partial \vec{V}\cdot\vec{t}}{\partial \vec{n}}\right|_l = \mu_v\left.\frac{\partial \vec{V}\cdot\vec{t}}{\partial \vec{n}}\right|_v \qquad (16\text{-b})$$

$$heating:\ k_l\left.\frac{\partial T}{\partial \vec{n}}\right|_l = k_v\left.\frac{\partial T}{\partial \vec{n}}\right|_v, \qquad (16\text{-c})$$

$$evaporation:\ T = T_{sat} \qquad (16\text{-d})$$

Air was used as the vapor for all of the simulations. The viscosity and thermal conductivity of air were lessened by an order of magnitude for selective cases, and were found not to change the results; therefore, the boundary condition at the interface is essentially a zero shear stress for all cases, and an insulated boundary for the heating cases.

As was noted before, the flow field is considered to be independent of the thermal field; therefore the flow field is first solved as a time-dependent solution, until a steady state solution has been reached. Once a steady-state solution has been reached, the energy equation is solved for both the fluid and solid regions, as a steady-state solution. The criteria used to determine a steady-state solution was when the mass flow rate out of the domain was within 0.05% of the mass flow rate into the domain for 0.05 seconds. The flow field was solved using the following procedure:

1. Solve momentum equations
2. Solve continuity (pressure correction) equation, update pressure and face mass flow rate
3. Repeat steps 1 and 2 until converged, for each time step

A co-located finite volume computational scheme, where both the flow-field variables and the pressure are stored in the cell centers, is used to solve the governing equations. The pressure is discretized in a manner similar to a staggered-grid scheme, while the pressure and velocity are coupled using the SIMPLE algorithm, described by Patankar [14]. All of the convective terms in the governing equations are discretized using a second-order upwind scheme.

The grid used for the numerical simulations consisted of rectangular shaped cells, which were produced in four axial layers in the liquid region, and one axial layer in the solid region. In the fluid region in the first layer, spanning from the disk surface to δ_{in}, there were 25 cell rows, with a growth rate of 1.01. The second layer, spanning from δ_{in} to $3\delta_{in}$, consisted of 30 cell rows with a growth rate of 1.02. The third layer, spanning from $3\delta_{in}$ to $10\delta_{in}$, consisted of 25 cell rows, and had a growth rate of 1.05. In the final layer, spanning from $10\delta_{in}$ to $100\delta_{in}$, there were 20 cell rows, with a growth rate of 1.2. In the solid region, there were 15 evenly spaced cell rows. In the radial direction, there were 15 evenly spaced cell columns between r_{in} and r_{hin}, and 75 evenly spaced cell columns between r_{hin} and r_{out}. The grid spans such a great distance in the axial direction ($100\delta_{in}$), because convergence is greatly increased with the added cells, so the computation actually runs more rapidly. A grid study was performed on a mesh that had 35 cell rows growing at a rate of 1.01 in the first layer of the liquid. The second layer had 40 cell rows with an aspect ratio of 1.02. The third layer had 25 cell rows with an aspect ratio of 1.075, and the fourth layer had 20 cells with an aspect ratio of 1.2. In the solid region there were 25 evenly spaced cell rows. In the radial direction, there were 15 cell columns between r_{in} and r_{hin}, and 100 evenly spaced cell columns between r_{hin} and r_{out}. The film thicknesses as well as the Nusselt numbers for both computational grids were within 0.1 percent of each other for all radial locations, for the 7 lpm, 100 rpm, 40°C case.

3 Results and Discussion

The disk has the same dimensions for all of the cases to simulate the experimental data of Ozar et al. (2004). The inner radius of the disk, r_{in}, is 0.0254 m. The inner radius of the heater, and the exit of the collar, r_{hin}, is 0.0508 m, while the outer radius of the heater, r_{hout}, is 0.18 m. The outer radius of the disk, r_{out}, is 0.2032 m. The aluminum disk thickness is 0.00635 m unless otherwise noted. The working fluid for all of the simulations is water. The thermal conductivity of aluminum is 202.4 W/m-K for all of the cases. This set-up is used to examine film thickness and heat transfer measurements for flow rates ranging from 3 to 15 lpm, and disk rotational speeds of 50 to 200 rpm. The effects of inlet temperature are considered by varying the inlet temperature between 20°C and 100°C. The effects of purely heating and evaporation are also presented. The purely heating boundary condition is used for the cases with inlet temperatures of 20°C and 40°C, and the evaporation boundary condition is used for cases with an inlet temperature of 100°C.

3.1 Film Dynamics

A prelude to the heat transfer characteristics of a controlled liquid impinging jet on a rotating surface is the fluid mechanics. In order to validate the present numerical schemes, the film thickness measurements are compared with experimental data obtained by two different techniques. The first technique, used by Thomas et al. [7], used a capacitance sensor. The present numerical results and the experimental results using the capacitance technique for the cases that matched the previously published data are presented in Figure 2. Since there were waves present on the surface of the liquid film in the experimental study, data were sampled at a rate of

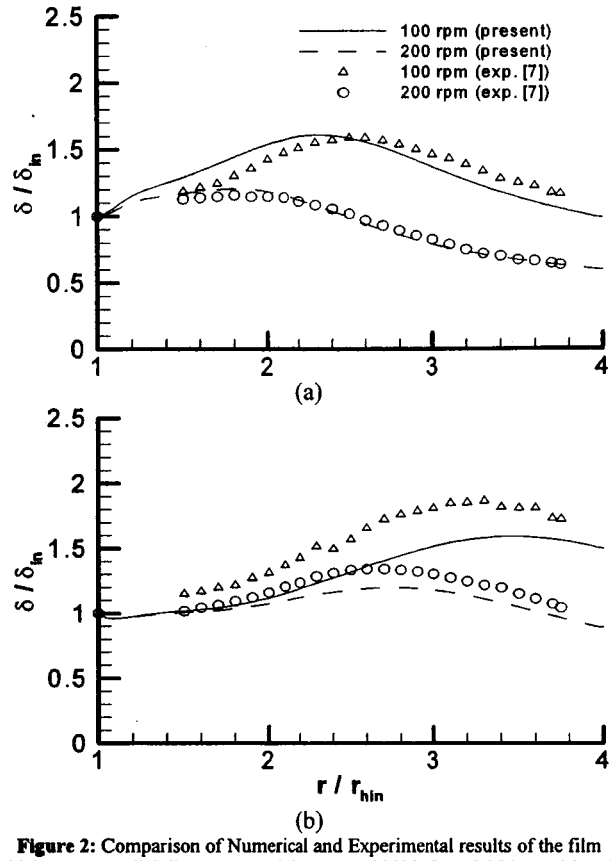

Figure 2: Comparison of Numerical and Experimental results of the film thickness vs. radial distance at an inlet temp of 20°C, δ_{in} = 0.254 mm (Num.) and 0.267 mm (exp.), and flow rates of (a) 7 lpm and (b) 15 lpm

one every two seconds, for every radial location, to obtain a repeatable average measurement. The maximum difference between the numerical and the experimental data for the 7 lpm, 100 and 200 rpm cases, and the 15 lpm, 100 and 200 rpm cases are 8.8, 3.9, 22.0 and 13.3 percent, respectively.

The present numerical film thickness measurements are also compared with experimental data obtained by Ozar et al. [15], in Figure 3. These experimental data were gathered by a laser light reflection technique, and images of the reflections of the dry and wet disk surfaces were digitally combined to obtain an image, which was post-processed to extract the center points of the reflections to determine the liquid film thickness. The slight wobbling of the disk was accounted for by triggering the camera at the same angular location. The final data points were fit with a least squares fourth-order polynomial. There is no mention of the repeatability of the published data, or variation with angular position. The numerical prediction tends to capture a thicker film thickness than the experimental predictions for the 3 and 7 lpm cases, for all of the presented rotational speeds. The opposite effect was observed for the 15 lpm cases. The differences may arise from modeling the flow as an axisymmetric geometry, which cannot capture surface waves.

The effects of flow rate, rotational speed and inlet temperature are displayed in Figure 4. The physical parameters that affect the flow are the inlet inertia of the impinging jet and the viscous interaction with the fluid and the disk. The viscous

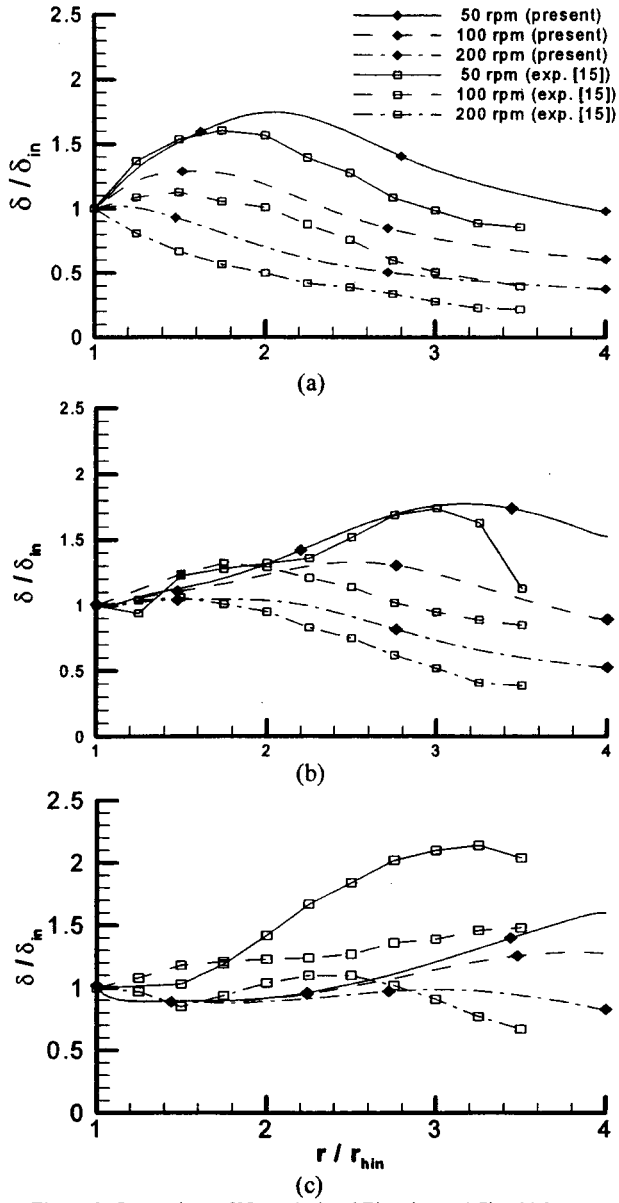

Figure 3: Comparison of Numerical and Experimental film thickness measurements vs. radial distance at 40°C inlet temperature, δ_{in} = 0.254 mm at flow rates of (a) 3 lpm (b) 7 lpm (c) 15 lpm

interaction between the disk and the liquid both retards the flow in the radial direction, and adds a centrifugal force because of the rotation of the disk. The film thickness generally increases due to the frictional losses of the fluid, and then decreases due to the centrifugal forces. The film thickness decreases with increasing rotational speed. Also the point where the maximum film thickness is located moves closer to the collar with increasing rotational speed. These two observed behaviors occur because the centrifugal force has an increased magnitude with increased rotational speed. The point of maximum film thickness moves closer to the outer edge of the disk as the flow rate is increased because the inertia of the fluid is greater, therefore taking a greater distance for the frictional forces of

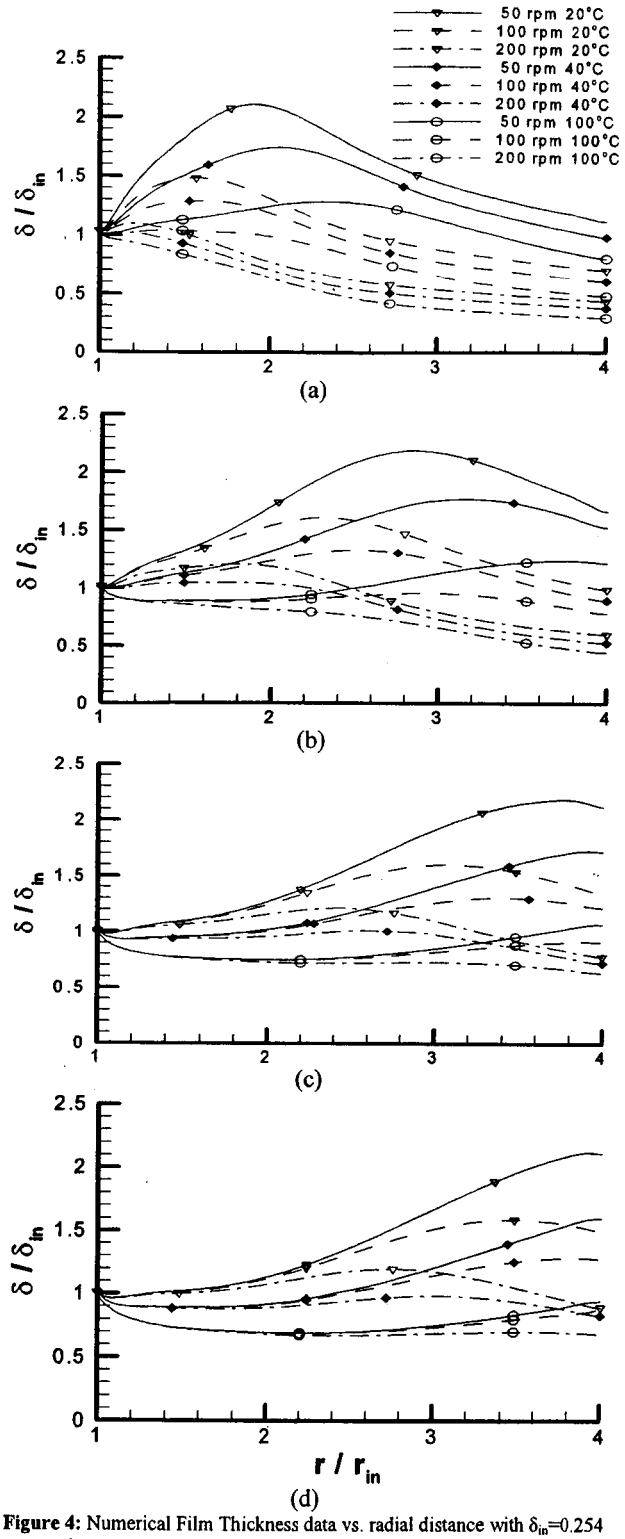

Figure 4: Numerical Film Thickness data vs. radial distance with δ_{in}=0.254 mm at various temperatures and flow rates of (a) 3 lpm (b) 7 lpm (c) 12 lpm (d) 15 lpm

the disk to retard the flow. A better indicator of when the centrifugal forces begin to influence the film thickness is to look at where the film thickness heights for the same flow rate

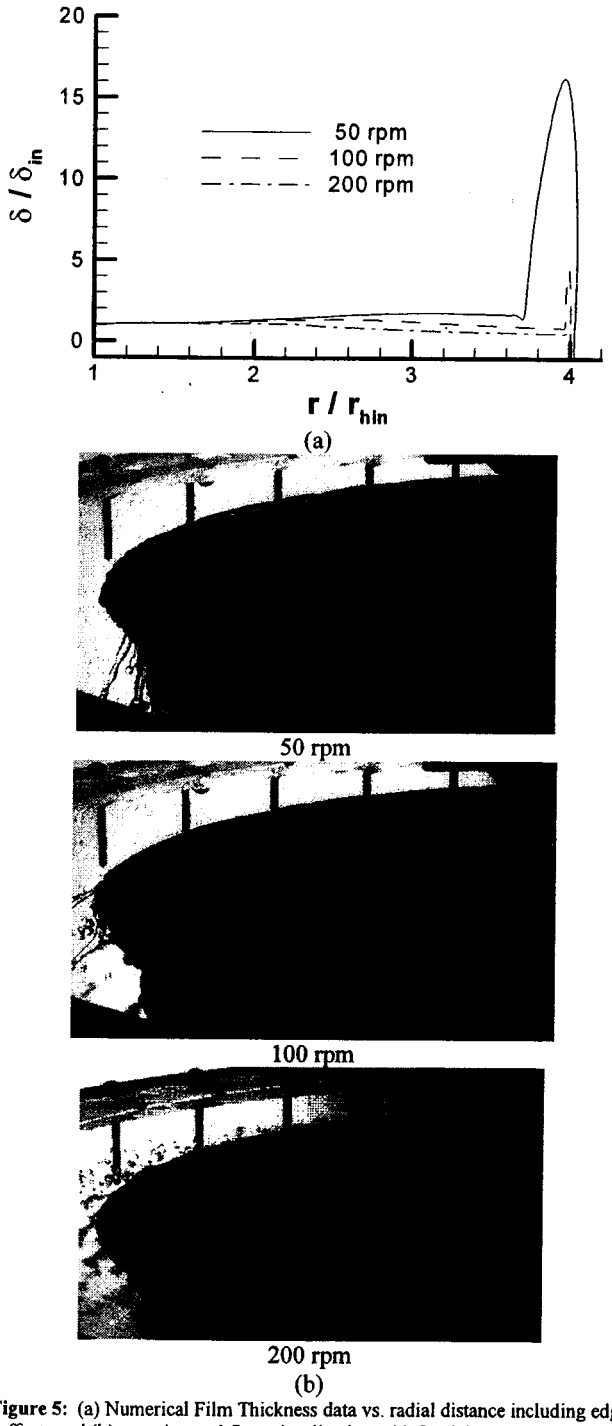

Figure 5: (a) Numerical Film Thickness data vs. radial distance including edge effects and (b) experimental flow visualization with δ_{in}=0.254 mm, 7 lpm and 40°C inlet temperature [15]

begin to vary with rotational speed. For the lower flow rates, rates there is a large amount of overlapping of the film thicknesses over the disk surface, and the distinction between the different rotational speeds is not realized until further out on the disk. The effects of increasing temperature tend to reduce the film thickness because the frictional losses are less due to the decrease in viscosity. Also, the point where the maximum film thickness occurs moves radially outward with increasing

temperature because the rotational effects from the rotation of the disk do not diffuse as readily to the bulk fluid movement with the decrease in viscosity.

Figure 5 illustrates the free surface shape when the edge effects are included in this analysis. The edge effects come from the fluid flowing over the edge of the disk, therefore causing a surface curvature. This surface curvature, raises the pressure because of the surface tension, and causes the fluid to make a lip at the disk's edge. This lip is commonly referred to as a "hydraulic jump". The film thickness of the model with the edge effects is within 2 percent of the model without the edge effects being modeled before a value of r/r_{hin} of 3.5. There is a hydraulic jump at the edge of the disk that decreases in magnitude as the rotational speed is increased. This result is qualitatively consistent with the edge effects observed by Ozar et al. [15]. The hydraulic jump at the edge of the disk is caused by the surface tension of the fluid. As the fluid flows over the edge, the surface curvature increases, therefore increasing the pressure. This increased pressure retards the flow and causes a jump. When rotational speeds are increased, the centrifugal forces increase, therefore making the edge effects have a relatively weaker resistance to the flow and washing off the hydraulic jump. It is important to note that there are surface waves present on the liquid film in the experiment that are not captured in the numerical model because of the axisymmetric assumption.

3.2 Thermal Characteristics

Now that an understanding of the liquid film flow characteristics is established, the heat transfer from the disk to the fluid can be investigated. Even though the conjugate effect is modeled, the Nusselt numbers are defined by the applied heat flux of the heater (Q/A), not the actual heat flux at the disk surface, and the temperature difference between the disk surface and the inlet temperature. This definition is used so that comparisons can be made with experimental data, in which only the heat flux at the heater is known. Figure 6 shows a comparison of local Nusselt numbers for various rotational speeds and flow rates of the present numerical simulation with the experimental data taken by Ozar et al. [10]. The numerical and experimental results correlate well at the larger radii, and increasingly poor at inner radii with increasing flow rate. The experimental Nusselt numbers at the inner radii are always lower than of the numerical results meaning that the surface temperatures at these locations are higher in the experiments. The differences may arise from non-uniform heating of the disk in the experiments because of the varying contact pressure of the heater. The contact pressure may vary because of the difference in coefficients of thermal expansion in the aluminum disk and the ceramic insulating layer.

The local Nusselt number versus radial location for various flow rates and rotational speeds are presented in Figure 7. The only variable in the definition of the local Nusselt number is the inverse of the temperature difference between the disk surface and the fluid inlet. The heater power for these cases is 4500 watts. The wall temperature starts off at the lowest value at the inlet of the impinging jet because the mean temperature of the fluid is the lowest at this point. As the mean temperature of the fluid increases as it flows and heats up over the disk, so does the disk's surface temperature. The conjugate

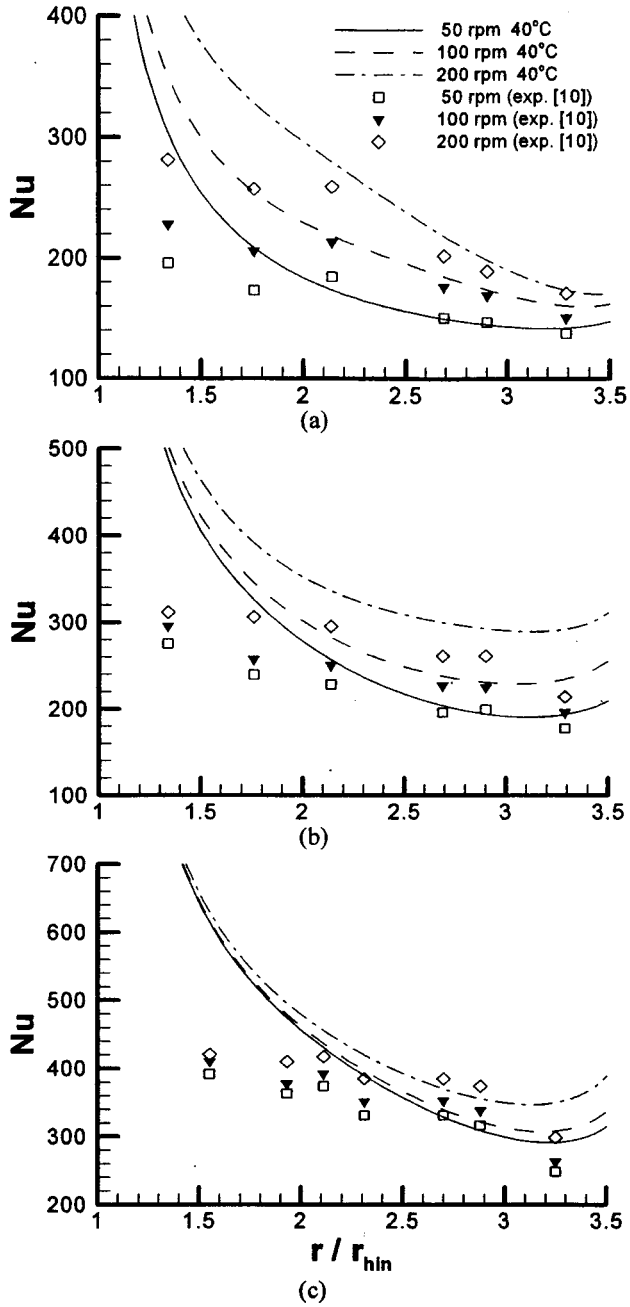

Figure 6: Comparison of Numerical and Experimental Local Nusselt Numbers vs. radial distance based on inlet temperature and radius with $\delta_{in} = 0.254$ mm, and an inlet temperature of 40°C for flow rates of (a) 3 lpm (b) 7 lpm (c) 15 lpm

heating effect is noticeable because the surface temperature actually decreases towards the end of the heater. The outer decrease in temperature occurs because of radial conduction within the disk. A more quantitative look at conjugate heating is discussed in the latter part of the thermal effects.

The surface temperature is also a function of the inlet flow rate, rotational speed, and inlet temperature. As the rotational speed increases, the surface temperature decreases, because the liquid film thickness decreases, which increases the

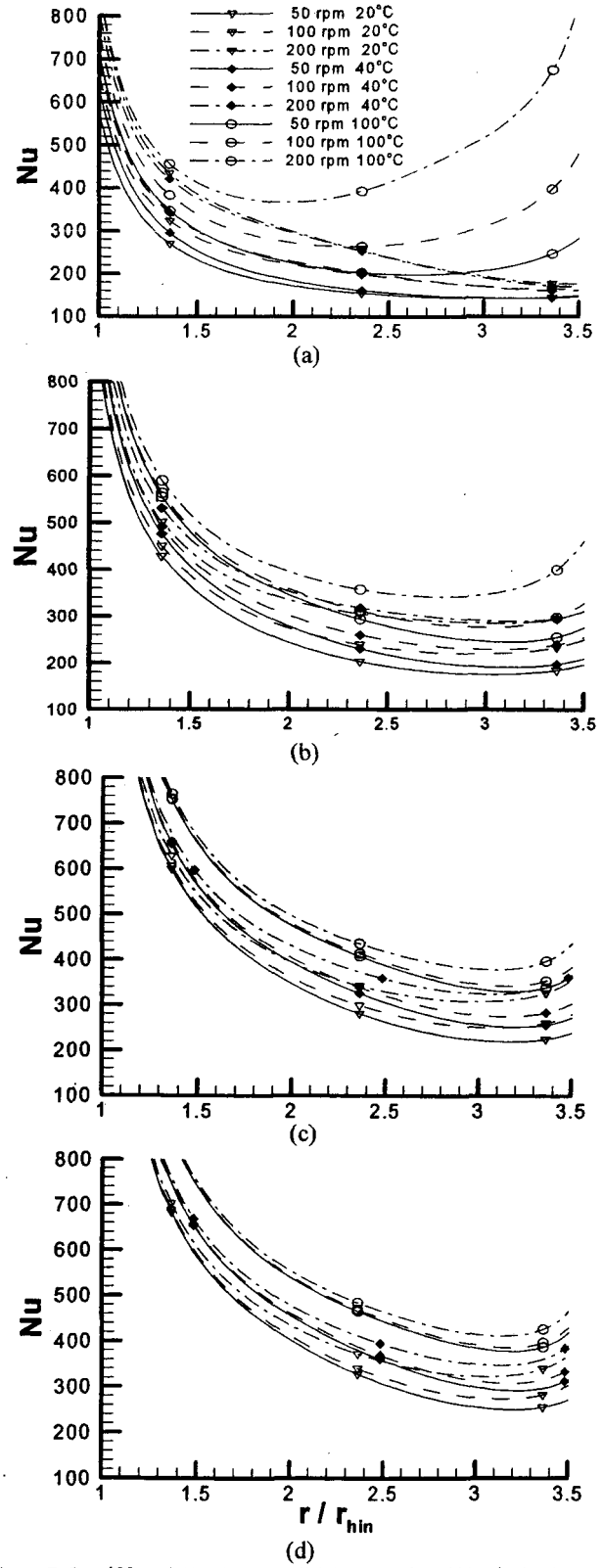

Figure 7: Local Nusselt Number vs. radial distance of liquid impinging jet on a rotating disk, δ_{in}=0.254 mm, and a heating power of 4500 watts (a) 3 lpm (b) 7 lpm (c) 12 lpm (d) 15 lpm

mean fluid velocity at each radial location. The surface temperature goes down with increasing flow rate, because the mean fluid temperature is lower. The increased inlet temperature decreases the viscosity, which thins the film. The fluid velocity is higher because of the thinner film, consequently decreasing the temperature difference between the disk and the inlet.

For the lower flow rates, the 20°C and 40°C inlet temperature cases show minimal difference in local Nusselt number, the differences are mainly seen with the increase in rotation. This result occurs because the fluid film characteristics are more strongly a function of rotational speed and than the liquid properties examined. At higher flow rates, the Nusselt Number distribution is affected more by temperature at the inner radii and more strongly by rotational speed at the outer radii. This trend physically occurs because the film characteristics vary more significantly with rotational speed at outer radii and vary more significantly with temperature at inner radii.

The effects of evaporation can be seen in the 100°C inlet temperature cases. The enhancement of heat transfer because of the evaporative effects are the most significant in the lower flow rate cases, and increase rapidly in these cases with rotational speed. This trend comes about because the thermal characteristics of the fluid resemble a fully developed thermal field at lesser radii for lower flow rates; therefore temperature profile throughout the film thickness is nearly linear. When the film thickness decreases, the surface temperature also decreases because temperature gradient throughout the liquid film remains constant. At higher flow rates, the flow is thermally developing throughout the heated region and has more of a parabolic temperature profile throughout the film thickness for most of the radii that are heated. Therefore, the evaporative cooling effects are less significant at higher flow rates. Heater powers of 2000 and 9000 watts were used to check the impact heater power had on the results. Even though the film temperature rose significantly, the Nusselt number remained within 0.5 percent for all of the evaporative cases that were run. The heater powers that are presently used are low enough that no nucleate boiling is expected to occur. The purely evaporative mode of mass transfer is observed in rotational cases under similar heating loads in experiments that are currently being run to observe the effects of boiling/evaporation.

The effects of inlet temperature, flow rate and rotational speed have been characterized for their affects on local Nusselt numbers. Now the overall heat transfer performance of the disk used in these numerical simulations are displayed by means of average Nusselt number versus flow rate in Figure 8. The data points are fit with a fourth order polynomial. It is very clear the overall heat transfer is increased with flow rate and with rotational speed. The overall heat transfer changes very little in the 20°C and 40°C inlet temperature cases, but increases significantly with the 100°C, evaporative case. The average Nusselt number increases nearly linearly with flow rate for the purely heating cases. For the evaporative case, this trend is different; the average Nusselt number is linear versus inlet flow rate for the low rotational

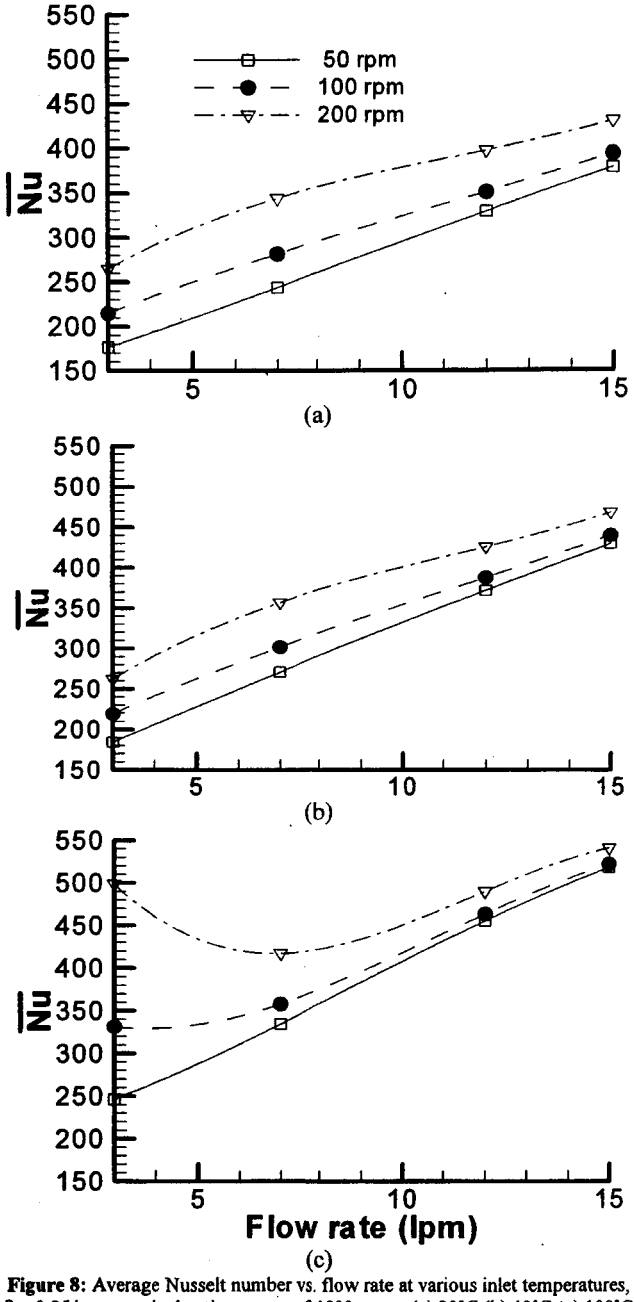

Figure 8: Average Nusselt number vs. flow rate at various inlet temperatures, δ_{in}=0.254 mm, and a heating power of 4500 watts (a) 20°C (b) 40°C (c) 100°C

speed cases and when the rotational speed is increased, a minimum overall heat transfer rate is observed at a slightly higher flow rate. The heat transfer is enhanced the most due to evaporative cooling at the lowest flow rates because of the nearly fully developed thermal field that exists.

The effects of the initial film thickness on the liquid film hydro and thermo characteristics are compared in Figure 9. The gap height used for all of the previous simulations was doubled and halved. The liquid film thickness behaves differently for the different gap heights in the inner inertia dominated region, and then the liquid film starts to behave similarly in the centrifugal dominated region. At the inner

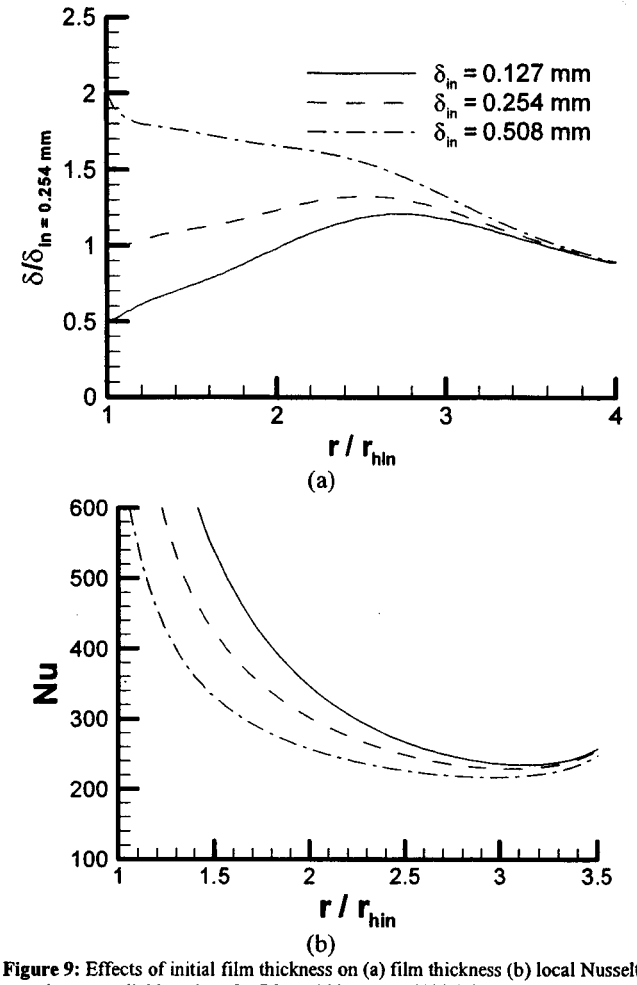

Figure 9: Effects of initial film thickness on (a) film thickness (b) local Nusselt number vs. radial location, for 7 lpm, 100 rpm, at 40°C inlet temperature case and 4500 watts.

radii, near the liquid impingement, the film thickness initially increases with the tighter gap height and decreases with the looser gap height. This effect is because the fluid velocity is higher for the tighter gap height, and also the characteristic length for the viscous diffusion is less, therefore making the frictional losses much greater, which decelerates the flow much more rapidly than the greater gap height. Once the initial inertia effects are lost due to friction and the centrifugal effects are gained, due to rotation, the film characteristics become independent of the initial thickness of the liquid and just a function of the flow rate and the rotational speed. The local Nusselt number shows a very similar trend to the initial film thickness. Initially, the local Nusselt number is greater for the tighter collar gap height, because the film velocity is greater. The opposite effect is seen for a looser gap height. The local Nusselt numbers tend to the same line at greater radii because the liquid film characteristics become very similar in this region.

The conjugate heating effect is quantified in Figure 10. The same cases were run with heating applied at the disk surface and at the bottom of the disk. The Nusselt numbers are within 10 percent with and without the conjugate effect for

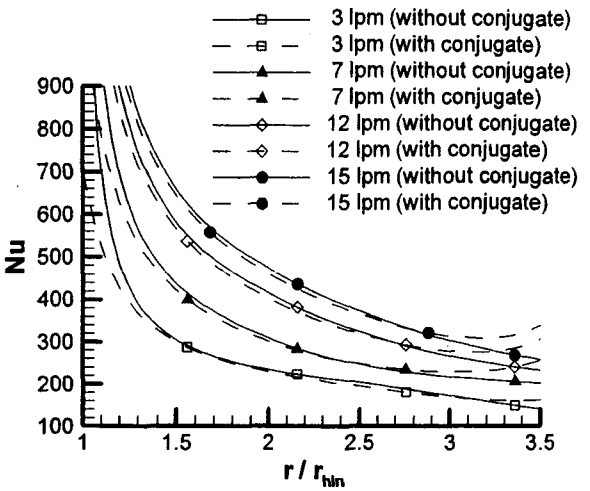

Figure 10: Conjugate effect on (a) local Nusselt number and (b) percent difference of local Nusselt Number vs. radial location for δ_{in} = 0.254 mm, and 40°C inlet, 4500 watts at 100 rpm for various flow rates.

about 80 percent of the disk. The conjugate effects are the greatest at the inner and outer radii, because of radial conduction through the disk. It is important to note that the average Nusselt numbers presented in this paper include the conjugate effect, and will be altered if the conjugate effect is not included. Also when the edge effects are modeled, the Nusselt number is within two percent of the model without the edge effects being modeled. The maximum difference in Nusselt number is at the outer edge of the heater because of the increased conjugate effect due to the convection heat transfer at the edge of the disk.

Doubling and halving the disk thickness examines the conjugate effect further. The effect of varying the disk thickness on Nusselt number is presented in Figure 11. The thicker the disk is, the more of an impact the conjugate effects has because of the increased cross-sectional area that allows radial conduction away from the heater. The Nusselt number is lower with increased disk thickness at the inner radii and higher at the outer radii. This happens because the fluid is being heated before the heater with conjugate heating, which

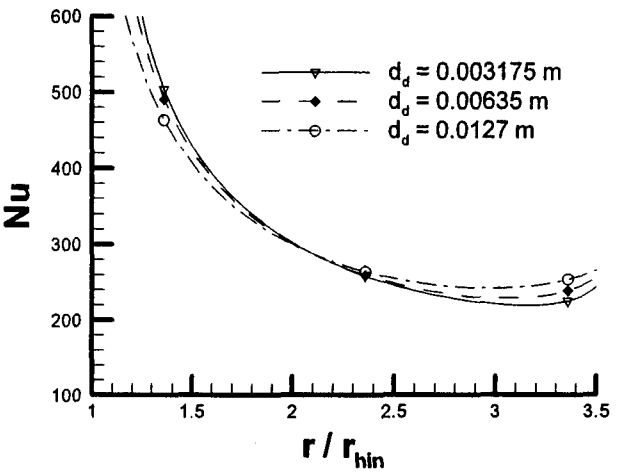

Figure 11: Conjugate effect on Nusselt number vs. radial location for various disk thickness at 7 lpm, 100 rpm, δ_{in} = 0.254 mm, and 40°C inlet, and 4500 watts.

increases the film temperature, and heated less at the end of the heater because heating power is lost at the outer radii of the disk.

The effect of surface tension was also studied in these numerical simulations, which could not be done with experiments, as there is no control of such physical parameters with any given fluid. The film thickness and local Nusselt numbers varied by less than 0.1 percent for all of the cases when the surface tension was reduced by half or doubled. The results are not presented because of redundancy.

3.3 Laminar to Turbulent transition

Since the flow field was considered to be in a laminar regime for all of the present cases, a discussion of this assumption is needed. Azuma and Hoshino [16] and Azuma [17] studied the laminar to turbulent transition characteristics on a stationary and rotating disk, respectively, of an impinging jet. In these studies the inlet Reynolds number, the nozzle height and radius were varied to examine the effects on the laminar to turbulent transition. These studies looked at the surface waves and made conclusions relating the classification of surface waves to the turbulence intensities. The first class of waves are 'D' waves, which form concentric circles on the disk, then the increased disturbance of the fluid changes these waves into lattice-shaped (LS) waves. Finally, these waves are disturbed even further and become sandpaper-like (SL) waves. The transition from a laminar film to a turbulent film is characterized when the LS waves turn into SL waves, and the SL waves cover more than 50 percent of the disk in the circumferential direction. Azuma and Hoshino [16] found in the stationary cases, a critical discharge Reynolds number, Re*, of 7.4×10^4. The discharge Reynolds number takes into account a discharge coefficient, c, which is a function of flow rate, density, nozzle diameter and nozzle gap height from the disk. The critical discharge Reynolds number only changed slightly with the rotational rates presently investigated and is why the stationary cases were used for comparison [17]. This Reynolds number is different from the Reynolds number, Re, defined by Ozar et al. [15], which incorporates the mass flow rate and inlet radius of

Table 1: Reynolds numbers, and laminar-turbulent transition radius from Azuma and Hoshino's (1984) analysis for the conditions considered in the present analysis.

Temp. (Celsius)	$\dot{V}$ (lpm)	c	Re	Re*	r_t^*	r_t/r_{hin}
20	3	0.61	156	1.3E+04	Laminar	Laminar
20	7	0.61	364	2.9E+04	Laminar	Laminar
20	12	0.61	624	5.0E+04	Laminar	Laminar
20	15	0.61	779	6.3E+04	Laminar	Laminar
40	3	0.61	246	2.0E+04	Laminar	Laminar
40	7	0.61	574	4.6E+04	Laminar	Laminar
40	12	0.61	984	7.9E+04	0.59	1.98
40	15	0.61	1230	9.9E+04	0.50	1.81
100	3	0.61	548	4.4E+04	Laminar	Laminar
100	7	0.61	1278	1.0E+05	0.49	1.79
100	12	0.61	2190	1.8E+05	0.35	1.53
100	15	0.61	2738	2.2E+05	0.30	1.42

the impinging jet.

The flow is considered laminar when the discharge Reynolds number is below the critical value. When the discharge Reynolds number is greater than the critical value, there is a radius of transition from laminar to turbulent flow at some radial location on the disk. There is a non-dimensional radius of transition, r_t^*, which is a function of the discharge Reynolds number, and the gap height and diameter of the nozzle. The Reynolds number, the discharge coefficient and the radius of transition, when applicable, are presented in Table 1. From this table, turbulence is only expected to influence the results of the higher flow rates and higher inlet fluid temperatures. Azuma [17] illustrated that the rotation tended to suppress the turbulent intensity when rotation was small (similar to rotational speeds used is this study), therefore pushing the transitional radius outward, and increase the turbulent intensity at higher rotational speed (rotational speeds greater than used in this study). It is important to note that the experiments were performed on a smooth glass disk, while the present numerical simulations are run on as laminar flow on an aluminum disk. Although laminar to turbulence transition is not considered in this numerical analysis, it is an area of interest for future research.

4 Conclusions

The liquid film characteristics studied in the range of 3 to 15 lpm, with disk rotational speeds of 50 to 200 rpm, and inlet temperatures varying from 20°C to 100°C are presented. The inertia of the fluid, the frictional losses as the liquid film flows over the disk and the centrifugal forces due to the rotation of the disk were all found to affect the film thickness. Some conclusions can be made about the fluid mechanics:

- The film thickness was found to decrease with increasing rotational speed. The transition point from the frictional loss dominated flow to the centrifugal force dominated flow was pushed radially outward with increasing flow rate.
- The increased inlet fluid temperature was found to decrease the film thickness because the frictional losses were less due to the decreased viscosity.
- The effect of the inlet gap height was found to effect the film thickness trend in the inner frictional loss dominated region but the film characteristics became similar once the centrifugal forces dominated the flow.

The heat transfer results were directly affected by the liquid film characteristics. Therefore, the heat transfer was affected by inlet temperature, inlet flow rate and the rotational speed. The conclusions that can be made about the heat transfer characteristics are:

- The heat transfer was enhanced with both increased rotational speed and increased flow rate. The enhancement of the heat transfer for the higher flow rate under increased rotational speed was not significant at inner radial distances.
- The increased temperature was found to increase the heat transfer because of the decreased film thickness.
- Evaporative effects were found to enhance the heat transfer more greatly at the lower flow rates, because the thermal field in the liquid film had fully developed characteristics closer the collar, therefore increasing the temperature gradient at the free surface, which enhances evaporative cooling.
- A reduced initial film thickness enhances the heat transfer at inner radial locations, but becomes less dependent on the inlet gap height radially outward on the disk, similar to the film characteristics.
- The conjugate effects made less than 10 percent difference in the local Nusselt in the middle of the heated section of the disk. However, the difference increased higher than 10 percent at the inner and outer 15 percent of the heated section of the disk.

From the above observations, when designing a system to utilize a controlled liquid impinging jet over a rotating surface, the point at which rotation starts to enhance the heat transfer varies with the inlet flow rate and rotational speed; this point is generally radially outward for the increase of these two parameters. From these observations, it is thought that for lower flow rates, smaller disks can be used, and still have the advantageous effects of rotation. On the other hand, for the higher flow rates and rotational speeds considered, a larger disk should be used to utilize the heat transfer enhancement due to rotation.

Acknowledgment

This work was sponsored by the NASA Microgravity Fluids Physics Program, Glenn Research Center, Cleveland Ohio, under the grant No. NCC3-789 with Dr. Subramanian Sankaran as the grant monitor.

References

[1] E.J. Watson, 1964, "The radial spread of a liquid jet over a horizontal plane," J. Fluid Mech., **20**, pp. 481-499.

[2] Z. H. Chaudhury, 1964, "Heat transfer in a radial liquid jet," J. Fluid Mech., **20,** pp. 501-511.

[3] A. D. D. Craik, R. C. Latham, M.J. Fawkes, and P.W.F. Gribbon, 1981, "The circular hydraulic jump," J. Fluid Mechanics, **112**, pp. 347-362.

[4] A.Y. Tong, 2003, "On the impingement heat transfer of an oblique free surface plane jet," Int. J. Heat and Mass Transfer, **46**, pp. 2077-2085.

[5] M.M. Rahman, A. Faghri, W.L. Hankey, and T.D. Swanson, 1990, "Computation of free surface flow of a liquid film at zero and normal gravity," Num. Heat Transfer, **17a**, pp. 53-71.

[6] A. Faghri, S. Thomas, M.M. Rahman, 1993, "Conjugate heat transfer from a heated disk to a thin liquid film formed by a controlled impinging jet," J. Heat Transfer, **115**, pp. 166-123.

[7] S. Thomas, A. Faghri, W. Hankey, 1991, "Experimental analysis and flow visualization of a thin liquid film on a stationary and rotating disk," Journal of Fluids Engineering, **133**, pp. 73-80.

[8] S. Thomas, W. Hankey, A. Faghri, T. Swanson, 1990, "One-dimensional analysis of the hydrodynamic and thermal characteristics of thin film flows including the hydraulic jump and rotation," J. Heat Transfer, **112**, pp. 728-735.

[9] M.M. Rahman, and A. Faghri, 1992, "Numerical simulation of fluid flow and heat transfer in a thin liquid film over a rotating disk," Int. J. Heat and Mass Transfer, **35**, pp. 1441-1453.

[10] B. Ozar, B.M. Cetegen, A. Faghri, 2004, "Experiments on heat transfer in a thin liquid film flowing over a rotating disk," J. Heat Transfer, **126**, pp. 184-192.

[11] C.W. Hirt and B.D. Nichols, 1981, "Volume of fluid (VOF) method for the dynamics of free boundaries," J. Comput. Phys., **39**, pp. 201-225.

[12] D.L. Youngs, 1982, "Time-dependent multimaterial flow with large fluid distortion," *Numerical Methods for Fluid Dynamics*, K.W. Morton and M.J. Baines, ed. Academic Press.

[13] J.U. Brackbill, D.B. Kothe and C. Zemach, 1992, "A continuum method for modeling surface tension", J. Comput. Phys., **100**, pp. 335-354.

[14] S.V. Patankar, 1980, *Numerical Heat Transfer and Fluid Flow*, Hemisphere, Washington, D.C.

[15] B. Ozar, B.M. Cetegen, A. Faghri, 2003, "Experiments on the flow of a thin liquid film over a horizontal stationary and rotating disk surface," Exp. in Fluids, **34**, pp. 556-565.

[16] T. Azuma and T. Hoshino, 1984, "The radial flow of a thin liquid film, 1st-4th Reports," *Bull JSME*, **27**, pp. 2739-2151.

[17] T. Azuma, 1989, "The transition from laminar to turbulent flow in the thin liquid film on a rotating disk," *Seventh Symposium on Turbulent Shear Flows*, Stanford University, Aug 21-23.

Submitted to J. Heat Transfer, April 2005

Analysis of hydrodynamics and heat transfer in a thin liquid film flowing over a rotating disk by integral method

by

S. Basu and B. M. Cetegen*

Mechanical Engineering Department

University of Connecticut, Storrs, CT 06269-3139

Abstract

An integral analysis of hydrodynamics and heat transfer in a thin liquid film flowing over a rotating disk surface is presented for both constant temperature and constant heat flux boundary conditions. The model is found to capture the correct trends of the liquid film thickness variation over the disk surface and compare reasonably well with experimental results over the range of Reynolds and Rossby numbers covering both inertia and rotation dominated regimes. Nusselt number variation over the disk surface shows two types of behavior. At low rotation rates, the Nusselt number exhibits a radial decay with Nusselt number magnitudes increasing with higher inlet Reynolds number for both constant wall temperature and heat flux cases. At high rotation rates, the Nusselt number profiles exhibit a peak whose location advances radially outward with increasing film Reynolds number or inertia. The results also compare favorably with the full numerical simulation results from an earlier study as well as with the reported experimental results.

Introduction

Many investigations have been performed in the past on flow and heat transfer characteristics in thin liquid films due to the fact that high heat transfer rates can be obtained in thin films as reviewed by Webb and Ma [1]. Hydrodynamic characteristics of thin liquid films flowing over stationary and rotating disk surfaces are important in understanding the major factors affecting the heat transfer performance. A better

* Corresponding author, Phone (860)486-2966, E-mail cetegen@engr.uconn.edu

understanding of the fluid mechanics of the liquid film flow allows better design and optimization of high performance compact heat transfer systems such as those employed in space applications, where considerations on efficiency, size, and weight are of critical importance. Study of rotating thin-film fluid physics and heat transfer is also of fundamental interest in the development of compact vapor absorption systems.

Watson [2] was first to analyze a free-falling jet impinging on a horizontal stationary plate. The film flow was divided into four regions. The first region was the impingement zone, followed by a second region of a growing boundary layer in the liquid film which eventually reaches to the film surface. Third region comprised of the transition to a fully developed film flow followed by a fully developed flow regime identified as the fourth region. For stationary and rotating liquid films at low flow rates and rotation speeds, a hydraulic jump could exist that has been studied both computationally and experimentally under normal and zero gravity conditions by Faghri and coworkers [3,4] and Avedisian and Zhao [5]. The hydraulic jump phenomenon was found to disappear at zero gravity conditions. Labus and Dewitt [6] conducted a combined numerical and experimental study to determine the free surface of a circular jet impinging on a flat plate in microgravity. The governing potential flow equations were solved numerically. The experimental study was performed using a drop-tower. The flow patterns of the free surface were examined experimentally, concluding that the surface tension and inertia were the dominant forces acting on the liquid. The experimental results were found to be in a good agreement with the numerical results. Thomas *et al.* [3] performed a useful one-dimensional analysis of the film thickness including the hydraulic jump phenomenon. They predicted significant thinning of the film with increased levels of rotation. They neglected inertia in their analysis.

Miyasaka [7] performed a similar theoretical and experimental study of the thickness of a thin viscous liquid film on a rotating disk. He obtained the film thickness by solving the governing equations of motion in the inviscid and viscous limits, with the latter utilizing the boundary layer approximation. Miyasaka also carried out experiments by using a liquid jet falling onto the center of a rotating disk. He deduced the film height from the electrical resistance of the liquid on the disk by comparing it to the electrical resistance of a standard thickness of the fluid. The computed values were found to agree

with the experimental results. Rahman *et al.* [4] was the first to report a full numerical solution of the momentum equations using a finite difference scheme. The method utilized a boundary-fitted coordinate gridding scheme with a k-ε model for turbulence closure and an iterative technique to define the free surface. They predicted the liquid-film thickness in the vicinity hydraulic jump reasonably well and evaluated the effects at the outer edge of the disk. Rahman and Faghri [8] investigated the hydrodynamic behavior of a thin liquid film flowing over a rotating disk. They used a three-dimensional boundary-fitted coordinate system to perform the calculations. The computed film thickness agreed well with existing experimental measurements. It was also concluded that the flow was dominated by inertia near the entrance and by centrifugal force near the outer edge the disk. The hydrodynamic characteristics of a radially spreading liquid jet on a horizontal plate were also predicted numerically by Buyevich and Ustinov [9]. However they reported no comparison with other studies.

Rao and Arakeri [10] performed an analytical study of free liquid jets on surfaces including circular plates, cones, and spheres. They used a boundary layer approximation and a third order polynomial for the velocity profile. The equations were solved by the integral method. Their work however did not include heat transfer in the film. Nevertheless, they were the first to use the integral approach to predict relevant parameters like film thickness. They also did not present any experimental validation of their data.

Azuma and Hoshino [11] examined the laminar-turbulent transition, liquid-film thickness, velocity profile, stability, and wall pressure fluctuations of thin liquid films on a stationary horizontal disk. The laminar-turbulent transition was determined as a function of the nozzle inside diameter, the gap height, and the volumetric flow rate. The liquid-film thickness measurements were performed using a needle probe. More recently, Ozar *et al.* [12] measured the liquid film thickness by a laser light reflection technique with which the spatial distributions of film thickness were captured including the hydraulic jump.

Heat transfer in liquid films was first analyzed by Chaudury [13] who incorporated Watson's results into the heat transfer analysis. Wang *et al.* [14] developed a two-domain solution in which the heat transfer at the liquid film and the solid disk were

treated separately and matched at the liquid-disk interface. Rahman and Faghri [8] used mixed numerical and analytical methods to predict the heat transfer. For developing flow and heat transfer, a three dimensional numerical model was utilized. Also, a two dimensional analytical solution was formulated for developing heat transfer and fully developed flow assuming solid body rotation. For the case of fully developed heat transfer and fluid flow, a closed form solution was developed. This solution predicted that the Nusselt number, based on film thickness, approached a constant value in the fully developed regime. Carper *et al.* [15] evaluated the convective heat transfer from a jet of cooling oil to an approximately isothermal rotating disk. Correlations were presented for the average Nusselt number as influenced by rotational Reynolds number, jet Reynolds number and radius of impingement. Carper *et al.* [16] later extended their study to include the effect of Prandtl numbers. Vader *et al.* [17] studied the effects of jet velocity and temperature on the heat transfer between a planar water jet and a stationary heated plate. They concluded that the heat transfer performance was affected by the free stream turbulence intensity and the Prandtl number. A similar study was presented by Stevens and Webb [18] where the influence of jet Reynolds number, nozzle to plate, spacing and jet diameter were evaluated. Empirical correlations were developed for stagnation point, local and average Nusselt numbers. Faghri *et al.* [19] presented heat transfer results for a controlled liquid impinging jet on a stationary disk. They presented a numerical study showing good agreement between heat transfer predictions and experimental data. Auone and Ramshaw [20] performed heat and mass transfer experiments on a liquid flowing over a rotating disk. They predicted the heat transfer coefficients analytically by adapting the solution that Nusselt [21] used for the film condensation under the influence of gravity. Ozar *et al.* [22] published an experimental study of heat transfer and reported the local and disk surface averaged Nusselt number over a range of flow rates and rotation speeds for water. Recently, Rice *et al.* [23] published full numerical computation of heat transfer in a thin liquid film over a rotating disk simulating the experimental conditions of Ozar *et al.* [22].

Review of the literature indicates that the analysis of the problem has progressed along two main themes. One theme has been numerical solution of the full problem taking into account its salient features. The other is of analytical nature utilizing

simplifying assumptions to obtain simple analytical results. In between lies the studies that utilize the Karman-Pohlhausen type integral analyses. This type of analysis is capable of capturing sufficient details of the solution while avoiding oversimplifications needed in analytical studies. For example, many of the analytical analyses had not considered the liquid film inertia effects in the presence of rotation. It was thus the objective of this study to present a comprehensive integral analysis of the thin liquid film flowing radially outward on a circular disk including effects of inertia and rotation. Capability of the integral method to predict the flow and heat transfer is demonstrated by comparisons with experimental and numerical results for the same problem.

Problem Formulation

The rotating disk is schematically shown in Fig. 1 which resembles the experimental set-up that has been utilized by Thomas *et al* [3] and Ozar *et al* [12,22] in a series of experimental studies. In the experiments, the flow is introduced from a central collar that directs the liquid radially outward over a gap height of h_o. The liquid flows over the rotating disk while being heated from underneath by an electric resistance heater. In these experimental studies, the liquid film thickness and heat transfer coefficients were measured. Liquid film thickness measurements were made by either a capacitance probe [3] or an optical technique [12]. The heat transfer coefficients were determined from the difference between the measured disk surface temperature and the liquid inlet temperatures and the constant heat flux supplied to the disk.

The problem is considered in the radial (r) and axial (z) coordinates assuming azimuthal symmetry. For this situation, the governing equations in cylindrical coordinate system over a rotating circular disk are:

Continuity: $$\frac{1}{r}\frac{\partial}{\partial r}(ru_r)+\frac{\partial u_z}{\partial z}=0 \qquad (1)$$

r-momentum: $$\frac{1}{r}\frac{\partial}{\partial r}(ru_ru_r)+\frac{\partial(u_ru_z)}{\partial z}=r\omega^2+\nu\left[\frac{\partial^2 u_r}{\partial z^2}-\frac{u_r}{r^2}+\frac{1}{r}\frac{\partial}{\partial r}\left(r\frac{\partial u_r}{\partial r}\right)\right] \qquad (2)$$

Energy: $$\frac{1}{r}\frac{\partial}{\partial r}[ru_rT]+\frac{\partial}{\partial z}[u_zT]=\alpha\left[\frac{1}{r}\frac{\partial}{\partial r}\left(r\frac{\partial T}{\partial r}\right)+\frac{\partial^2 T}{\partial z^2}\right] \qquad (3)$$

Defining non-dimensional parameters as,

$$\tilde{r} \equiv \frac{r}{r_0}, \tilde{u}_r \equiv \frac{u_r}{u_o}, \tilde{z} \equiv \frac{z}{h_o}, \tilde{u}_z \equiv \frac{u_z}{u_o}, \theta_T \equiv \frac{T - T_o}{T_o - T_i}, \theta_q \equiv \left(\frac{k}{q_o h_o}\right)(T - T_i),$$

where r_0 is the inlet radius of the disk, u_0 is the inlet velocity of the liquid jet, h_0 is the collar height, θ_T is the nondimensional temperature for the constant wall temperature and θ_q is its counterpart for constant wall heat flux. T_0 is the temperature of the disk surface for constant wall temperature case, T_i is the inlet temperature of the liquid jet, q_0 is the heat flux supplied to the disk for the constant wall heat flux case. Non-dimensionalizing the governing equations we obtain,

$$\frac{1}{\tilde{r}}\frac{\partial}{\partial \tilde{r}}(\tilde{r}\tilde{u}_r) + \left(\frac{r_o}{h_o}\right)\frac{\partial \tilde{u}_z}{\partial \tilde{z}} = 0 \tag{4}$$

$$\frac{1}{\tilde{r}}\frac{\partial}{\partial \tilde{r}}[\tilde{r}\tilde{u}_r^2] + \left(\frac{r_o}{h_o}\right)\frac{\partial}{\partial \tilde{z}}[\tilde{u}_r\tilde{u}_z] = \frac{\tilde{r}}{Ro} + \frac{1}{\mathrm{Re}}\left[\frac{1}{\tilde{r}}\frac{\partial}{\partial \tilde{r}}\left(\tilde{r}\frac{\partial \tilde{u}_r}{\partial \tilde{r}}\right) + \left(\frac{r_o}{h_o}\right)^2\frac{\partial^2 \tilde{u}_r}{\partial \tilde{z}^2} - \frac{\tilde{u}_r}{\tilde{r}^2}\right] \tag{5}$$

$$\frac{1}{\tilde{r}}\frac{\partial}{\partial \tilde{r}}[\tilde{r}\tilde{u}_r\theta] + \left(\frac{r_o}{h_o}\right)\frac{\partial}{\partial \tilde{z}}[\tilde{u}_z\theta] = \frac{1}{Pe}\left[\frac{1}{\tilde{r}}\frac{\partial}{\partial \tilde{r}}\left(\tilde{r}\frac{\partial \theta}{\partial \tilde{r}}\right) + \left(\frac{r_o}{h_o}\right)^2\frac{\partial^2 \theta}{\partial \tilde{z}^2}\right] \tag{6}$$

where Reynolds, Rossby and Peclet numbers are defined as

$$\mathrm{Re} \equiv \frac{u_o r_o}{\nu}, Ro \equiv \frac{u_o^2}{\omega^2 r_o^2}, Pe \equiv \frac{u_o r_o}{\alpha}$$

where ν is the kinematic viscosity and α is the thermal diffusivity, both of which are assumed to be constant in the context of this analysis.

Since $r_o > h_o$, then, $\frac{r_o^2}{h_o^2} >> 1$, we can infer that

$$\left(\frac{r_o}{h_o}\right)^2\frac{\partial^2 \tilde{u}_r}{\partial \tilde{z}^2} >> \frac{1}{\tilde{r}}\frac{\partial}{\partial \tilde{r}}\left(\tilde{r}\frac{\partial \tilde{u}_r}{\partial \tilde{r}}\right) \text{and} \left(\frac{r_o}{h_o}\right)^2\frac{\partial^2 \tilde{u}_r}{\partial \tilde{z}^2} >> \frac{\tilde{u}_r}{\tilde{r}^2} \text{and} \left(\frac{r_o}{h_o}\right)^2\frac{\partial^2 \theta}{\partial \tilde{z}^2} >> \frac{1}{\tilde{r}}\frac{\partial}{\partial \tilde{r}}\left(\tilde{r}\frac{\partial \theta}{\partial \tilde{r}}\right)$$

Hence the momentum and energy equations take the form

$$\frac{1}{\tilde{r}}\frac{\partial}{\partial \tilde{r}}[\tilde{r}\tilde{u}_r^2] + \left(\frac{r_o}{h_o}\right)\frac{\partial}{\partial \tilde{z}}[\tilde{u}_r\tilde{u}_z] = \frac{\tilde{r}}{Ro} + \frac{1}{\mathrm{Re}}\left[\left(\frac{r_o}{h_o}\right)^2\frac{\partial^2 \tilde{u}_r}{\partial \tilde{z}^2}\right] \tag{7}$$

$$\frac{1}{\tilde{r}}\frac{\partial}{\partial \tilde{r}}[\tilde{r}\tilde{u}_r\theta] + \left(\frac{r_o}{h_o}\right)\frac{\partial}{\partial \tilde{z}}[\tilde{u}_z\theta] = \frac{1}{Pe}\left(\frac{r_o}{h_o}\right)^2\frac{\partial^2 \theta}{\partial \tilde{z}^2} \tag{8}$$

Liquid Film Hydrodynamics

Integrating the momentum equation with respect to $\tilde{z}$ from 0 to $\tilde{\delta} = \frac{\delta}{h_o}$, we get,

$$\frac{1}{\tilde{r}}\frac{\partial}{\partial \tilde{r}}\int_0^{\tilde{\delta}} \tilde{r}\tilde{u}_r^2 d\tilde{z} + \frac{r_o}{h_o}[\tilde{u}_r\tilde{u}_z]_{\tilde{\delta}} = \frac{\tilde{r}\tilde{\delta}}{Ro} - \frac{1}{\mathrm{Re}}\left[\left(\frac{r_o}{h_o}\right)^2 \frac{\partial \tilde{u}_r}{\partial \tilde{z}}\bigg|_0\right] \tag{9}$$

From continuity equation, we can write

$$\tilde{u}_z(\tilde{\delta}) = -\frac{h_o}{r_o\tilde{r}}\frac{\partial}{\partial \tilde{r}}\int_0^{\tilde{\delta}} \tilde{r}\tilde{u}_r d\tilde{z} \tag{10}$$

A parabolic radial velocity profile is assumed as,

$$\tilde{u}_r = a_0 + a_1\tilde{z} + a_2\tilde{z}^2 \tag{11}$$

subject to the boundary conditions of no slip at the wall $\tilde{u}_r(\tilde{z}=0)=0$ and no shear at the free surface $\frac{\partial \tilde{u}_r}{\partial \tilde{z}}(\tilde{z}=\tilde{\delta})=0$. In addition, the total volume flow at any cross-section perpendicular to r has to be equal to the inlet flow rate for the case of no vaporization or mass loss, these conditions allow determination of coefficients in the velocity profile leading to,

$$\tilde{u}_r = 3\left(\frac{\tilde{z}}{\tilde{r}\tilde{\delta}^2}\right) - \frac{3}{2}\left(\frac{\tilde{z}^2}{\tilde{r}\tilde{\delta}^3}\right) \tag{12}$$

Substituting this profile into the integral momentum equation and integrating with respect to z, one gets

$$\frac{d\tilde{\delta}}{d\tilde{r}} + \frac{\tilde{\delta}}{\tilde{r}} + \frac{5}{6Ro}\tilde{r}^3\tilde{\delta}^3 = \frac{5}{2\mathrm{Re}}\left(\frac{r_o}{h_o}\right)^2\tilde{r} \tag{13}$$

In this equation, the first two terms are due to advection, the third term is a result of rotation and the term on the right side represents the viscous shear. Equation 13 subject to the initial condition $\tilde{\delta}(\tilde{r}=1)=1$ was numerically integrated to determine the film thickness over the disk surface. Equation (13) becomes an algebraic equation for the case of negligible inertia in which case the first two terms disappear. The film thickness can be written in exact form as,

$$\tilde{\delta} = \left[\frac{3Ro}{\mathrm{Re}}\left(\frac{r_o}{h_o}\right)^2\right]^{1/3}\frac{1}{\tilde{r}^{2/3}} \tag{14}$$

This result is identical to that obtained based on the falling film analysis with gravity being replaced by the centrifugal force. Having the liquid film hydrodynamics established, we now proceed with the heat transfer analysis in the film.

Heat Transfer in the Liquid Film

The heat transfer in the liquid film is analyzed by considering the two cases of constant disk surface temperature and constant disk surface heat flux. In either case, there is a thermal entry region where the thermal boundary layer lies below the film surface as shown in Fig. 1. As it is shown in Appendix A for constant disk surface temperature case, the thermal entry region length scales as,

$$\tilde{r}_* = \left[1 + \frac{Pe}{6}\left(\frac{h_o}{r_o}\right)^2\right]^{1/2} \tag{15}$$

For moderate Peclet numbers, $\tilde{r}_* \approx 1$ *(or* $r_* \approx r_o$*)* since $h_o << r_o$, thus allowing us to neglect the entry length.

Constant disk surface temperature case

For this case, the temperature profile can be constructed as a second order polynomial given by,

$$\theta = a_0 + a_1\left(\frac{z}{\delta_T}\right) + a_2\left(\frac{z}{\delta_T}\right)^2 \tag{16}$$

which has to satisfy the boundary conditions: $\theta = 0$ at $z = 0$, $\frac{d\theta}{dz} = 0$ at $z = \delta_T$. The profile satisfying these conditions is,

$$\theta = \theta_\infty\left[\left(\frac{z}{\delta_T}\right)^2 - 2\left(\frac{z}{\delta_T}\right)\right] \quad \text{where} \quad \begin{array}{l} \delta_T < \delta \Rightarrow \theta_\infty = 1 \\ \delta_T = \delta \Rightarrow \theta_\infty = \dfrac{T_\delta(r) - T_o}{T_o - T_i} \end{array} \tag{17}$$

Substituting this profile along with the velocity profile into the integral energy equation, one obtains,

$$\frac{d\theta_\infty}{d\tilde{r}} = -\theta_\infty\left[\frac{5}{2Pe}\left(\frac{r_o}{h_o}\right)^2\frac{\tilde{r}}{\tilde{\delta}} - \frac{5}{4}\frac{d\tilde{\delta}}{d\tilde{r}}\right] \tag{18}$$

Integrating and applying the condition that $\theta_\infty(\tilde{r} = \tilde{r}_*) = 1$, we get

$$\theta_\infty = \exp\left[-\frac{5}{2}\left(\frac{r_o}{h_o}\right)^2 \frac{1}{Pe}\int_{r_*}^{\tilde{r}} \frac{\tilde{r}d\tilde{r}}{\tilde{\delta}} + \frac{5}{4}(\tilde{\delta} - \tilde{\delta}_*)\right] \tag{19}$$

Defining the Nusselt number as, $Nu_T \equiv \frac{hr_0}{k} = -\frac{r_o}{\tilde{\delta}}\frac{d\theta}{d\tilde{z}}\bigg|_{\tilde{z}=0}$

$$Nu_T = 2\frac{r_o}{h_o\tilde{\delta}}\exp\left[-\frac{5}{2}\left(\frac{r_0}{h_0}\right)^2 \frac{1}{Pe}\int_{r_*}^{\tilde{r}} \frac{\tilde{r}d\tilde{r}}{\tilde{\delta}} + \frac{5}{4}(\tilde{\delta} - \tilde{\delta}_*)\right] \tag{20}$$

The area-averaged Nusselt number can be defined as

$$Nu_{avg} = \frac{1}{\pi(\tilde{r}^2 - 1)}\int_1^{\tilde{r}} Nu_T 2\pi\tilde{r}d\tilde{r} \tag{21}$$

Constant heat flux case:

The temperature profile for the constant heat flux case is subject to $\frac{d\theta_q}{d\tilde{z}}\bigg|_{\tilde{z}=0} = -1$ and $\frac{d\theta_q}{d\tilde{z}}\bigg|_{\tilde{z}=\tilde{\delta}} = 0$, i.e., prescribed heat flux at the wall, q_o and adiabatic free surface. With these conditions, the temperature profile becomes,

$$\theta = a_o + \tilde{\delta}\left(\frac{\hat{z}^2}{2} - \hat{z}\right) \tag{22}$$

where a_0 is a parameter which is a function of r. Substituting this temperature profile into the integral form of the energy equation and integrating, one gets,

$$\frac{da_0}{d\tilde{r}} + a_0\frac{d\tilde{\delta}}{d\tilde{r}} = \frac{\tilde{r}}{Pe}\left(\frac{r_0}{h_0}\right)^2 + \frac{2}{5}\frac{d\tilde{\delta}}{d\tilde{r}} + \frac{\tilde{\delta}}{2}\frac{d\tilde{\delta}}{d\tilde{r}} \tag{23}$$

subject to the initial value of $a_0(\tilde{r}=1)$. While this value can be taken as $a_o(\tilde{r})=1$ based on $\theta_q(\tilde{r}=1)=1$ in eqn. (22), a better estimate is provided by integrating the energy flux at $\tilde{r}=1$, $\int_0^1\left[\frac{q_o h_o\theta_q}{kT_i}+1\right]d\tilde{z}=1$, yielding $a_o(\tilde{r}=1)=1/3$. For the case of negligible inertia, an analytical solution for a_o can be obtained as described in Appendix B,

$$a_o = \left(\frac{r_o}{h_o}\right)^2\frac{\tilde{r}-1}{RePr} - \frac{7}{20}\left(\frac{r_o}{h_o}\right)^{2/3}\left(\frac{3Ro}{Re}\right)^{1/3}(\tilde{r}^{-2/3}-1) + \frac{1}{3} \tag{24}$$

Nusselt number for the case of constant disk surface heat flux can be found from,

$$Nu_q \equiv \frac{hr_o}{k} = \frac{q_o r_o}{k[T(\tilde{z}=0) - T_i]} = \frac{r_o}{a_o h_o} \tag{25}$$

For the case of negligible inertia,

$$Nu_q = \left[\left(\frac{r_o}{h_o}\right)\frac{\tilde{r}-1}{RePr} - \frac{3^{1/3}7}{20}\left(\frac{r_o}{h_o}\right)^{-1/3}\left(\frac{Ro}{Re}\right)^{1/3}(\tilde{r}^{-2/3}-1) + \frac{1}{3}\left(\frac{h_o}{r_o}\right)\right]^{-1} \tag{26}$$

The averaged Nusselt number is obtained by integrating the local Nusselt number over the disk surface based on eqn. (21). In the following, the results obtained from this analysis are presented and discussed.

Results and Discussion

The calculation of the liquid film thickness and Nusselt numbers for constant wall temperature and constant heat flux cases were performed for a range of inlet Reynolds numbers $\mathrm{Re} \equiv \frac{u_o r_o}{\nu}$ and Rossby numbers $Ro \equiv \frac{u_o^2}{\omega^2 r_o^2}$. The range of parameters were chosen to cover those reported in the experiments of Ozar *et al* [12,22] and the recent numerical simulations of Rice *et al* [23]. The value of the geometric parameter $\frac{r_o}{h_o}$ was taken to be same as in the experiments with a value of 200. In the following, the computed results are presented and compared with numerical and experimental results mentioned above.

Figure 2 shows the variation of the film thickness over the disk surface with Reynolds number for two values of Rossby number. At low rotation speeds (Ro = 1000), the film thickness initially increases along the disk radius and then begins to thin out at outer radii due to effect of rotation as seen in Fig. 2a. The film thickness decreases with increasing inlet velocity or Reynolds number and the peak film thickness location shifts to larger radii with increasing Re. The analytical result given by eqn. (14) is also shown in Fig. 2a for Re = 10^4. It is seen that the two results agree at large radii where the inertial effects are diminished and the negligible inertia result agrees with the full solution. At high rotation rates (Ro = 0.5), film thickness exhibits a radial decay with the film thickness still decreasing with increasing inertia as shown in Fig. 2b. The variation

of the film thickness for high levels of rotation is well represented by eqn. (14) as seen by the agreement at Re = 10^4. The effect of varying the rotation speed on the film thickness at a constant value of inlet velocity or Reynolds number is depicted in Fig. 3. With increasing rotation speed (i.e. decreasing Ro), the film thickness decreases. The trend at high Ro, which exhibits a maximum in the film thickness, gradually changes to a radially decaying film thickness at high rotation speeds (i.e. low Ro). This change appears to happen at around Ro = 10 for this case. The computed results are in reasonably good agreement with the experimental results reported by Ozar et al [22] as shown in Fig. 4. The integral model captures the trend of liquid film thickness variation at different Reynolds and Rossby numbers. Due to the uncertainties in the experimentally measured film thickness, a closer agreement can not be expected.

Figure 5 shows the variation of the Nusselt number over the disk surface for the case of constant wall temperature. At low rotation rates (Ro = 1000), shown in Fig. 5a, the Nusselt number decreases continuously with increasing radial distance. The magnitude of Nusselt number is highest at the entrance since the temperature gradient, and heat flux is the highest there at the liquid-disk interface. With increasing radial distance, the liquid film temperature increases and consequently the heat flux diminishes leading to a decrease in the heat transfer coefficient and Nusselt number. The value of Nusselt number approaches a constant value at large radii. Nusselt number increases with increasing inlet velocity or Reynolds number as expected. At high rotation speeds, shown in Fig. 5b, the trend of Nusselt number is quite different in that it increases from the inlet to a maximum value and decreases from that point on. The magnitude of Nusselt number increases with increasing Reynolds number with the peak Nusselt number location shifting radially outward. This prounounced increase in Nusselt number is due to the thinning of the liquid film due to inertia and rotation. The decrease at larger radii is due to the effect of heating of the liquid film reducing the temperature gradient and heat flux. At high rotation rates, Nusselt number increases significantly above the values for low rotation rates suggesting the strong enhancement of heat transfer due to rotation.

To better visualize the effects of rotation at a fixed value of inlet velocity or Reynolds number, Figure 6 shows the effect of Rossby number on Nusselt number

variation. At low rotation speeds (i.e. high Ro), the Nusselt number is highest at the entrance and decreases with increasing radial distance. At about Ro = 1, the trend exhibits an increase of Nusselt number from the inlet reaching a maximum value followed by a decay. At higher rotation rates (Ro = 0.5), this trend of Nusselt number becomes more pronounced with the maximum values of Nusselt number being an order of magnitude higher. The peak Nusselt number location shifts to smaller radii indicating that the rotational effects are felt at smaller radii with increasing rotation speed.

In Figure 7, the results are shown for the constant heat flux case at two values of Rossby number. At low rotation rates (i.e. high Ro), the Nusselt number variation is similar to that of constant wall temperature case (shown in Fig. 5a) except that the Nusselt number magnitude is higher than that for the constant wall temperature. The increase in Nusselt number is expected since the heat flux at the disk surface is maintained in this case. For the high rotation speed (Ro = 0.5), Nusselt number exhibits a decay with increasing radial distance at low Reynolds number as the temperature of the liquid at the disk surface increases with increasing radial distance, similar to the constant wall temperature case. With increasing Reynolds number, the Nusselt number magnitude increases and it exhibits a maximum.

Figure 8 illustrates the influence of rotation on the Nusselt number variation with at a fixed value of inlet velocity or Reynolds number. It is found that rotation enhances the heat transfer into the liquid film very significantly. As the rotation rate reduces, the maximum in the Nusselt number variation disappears and it decays continuously with increasing radial distance. The location of the peak shifts to smaller radii with increasing rotation rate (i.e. decreasing Ro) since the effects of rotation are felt further in with increasing rotation.

Figure 9 shows the comparison of the integral method results with the full numerical simulation results of Rice *et al* [23]. The comparisons are shown for Re = 1.42 10^4 and 2.84 10^4 for two rotation speeds of 50 and 100 rpm. The agreement between the integral model and numerical simulations appears to be good with maximum deviations of about 20 %. It is conceivable that the differences are due to variable fluid properties not accounted for in the integral model as well as the more detailed treatment afforded in the numerical model, such as conjugate heat transfer, evaporation effects etc. Figure 10

displays the comparison of experimental results with the integral model for two cases. It is found that the experimental results good agreement with the model for these two cases with the radial variation of experimental Nusselt number being slightly less. Considering the uncertainty of the experimental data and the simplifications employed in the model, the level of agreement is remarkable.

The area averaged Nusselt numbers over the disk surface are shown in Figs. 11 and 12 respectively for the cases of constant wall temperature and constant heat flux. The trend of average Nusselt number is approximately linear for both cases with slightly decreasing curvature for the constant wall heat flux at low rotation rates (i.e. high Ro). The influence of Rossby number is nonlinear however and the average Nusselt number is found to scale as $\overline{Nu} \propto Ro^{-m}$ where $m \approx 0.55$ for constant wall temperature and $m \approx 0.18$ for constant heat flux. The stronger dependence for constant wall temperature can be rationalized based on the fact that heat transfer into the film is enhanced more for the constant wall temperature case in contrast to the constant wall heat flux.

Finally, Figure 13 shows the comparison of the analytical solution given by eqn. (26) for the negligible inertia case with the full solution for Re = 10^4 and Ro = 0.5. It is seen that the two solutions differ substantially near the entrance region, but merge at large radii where the inertial effects have diminished.

Concluding Remarks

A detailed integral analysis of flow and heat transfer in a thin liquid film flowing over a rotating disk was formulated to determine the liquid film thickness and Nusselt numbers for both constant wall temperature and heat flux cases. The results are presented for a range of inlet liquid flow rates or Reynolds numbers and Rossby numbers. It is found that the integral model captures the variation of film thickness over the disk radius for a range of parameters representing both inertia and rotation dominated regimes. At low rotation rates corresponding to high Rossby numbers, the film thickness grows radially until the centrifugal effect becomes sufficiently strong at large radii. For high inlet flow rates or Reynolds numbers, the film thickness decreases radially with decay being stronger with increasing inertia. For low inertia, the film thickness increases radially due to significant retardation of the film flow by viscosity. In cases where both

inertial and rotational effects come into play, the film thickness first increases reaching a maximum followed by radial decay. The location of maximum film thickness changes based on the values of Reynolds and Rossby numbers. For cases dominated either by high rotation or low inertia, the film thickness is well represented by the analytical expression obtained for negligible inertia.

The analysis of the heat transfer in the liquid film indicate that the Nusselt number exhibits a radial decay at low rotation rates (i.e. high Ro) for both cases of constant wall temperature and constant heat flux. The magnitude of Nusselt number is linearly dependent on inlet Reynolds number for both cases. However, the Nusselt number values for constant wall heat flux are greater than those for the constant wall temperature. At high rotation speeds and inlet Reynolds numbers, the Nusselt number first increases, reaches a peak and then displays a radial decay. The radial location of the peak Nusselt number shifts to larger radii with increasing Reynolds number and this is due to the competing effects of inertia and rotation on the film thickness and heat transfer characteristics. Effect of Rossby number appears to be significantly non-linear and high rotation rates can produce significant enhancement in heat transfer for both cases of constant wall temperature and heat flux. In addition to local Nusselt number variation, the disk surface area averaged Nusselt numbers were computed for both cases. They also show an approximately linear variation with respect to inlet flow rate or Reynolds number and inverse power law dependence on Rossby number. Rossby number dependence is stronger for the constant wall temperature case.

The results obtained from this integral analysis were compared with those from a recent numerical study of Rice *et al* [23] as well as the experiments of Ozar *et al* [21,22]. Both comparisons indicate good agreement with the integral model. Finally, the integral analysis provided analytical and semi-analytical expressions for the local Nusselt number in the limit of negligible inertia for the cases of constant wall heat flux and constant wall temperature respectively.

Acknowledgments

The work presented in this article was funded by NASA Microgravity Fluid Physics Program under Grant No. NCC3-789 with Dr. S. Sankaran as the grant monitor.

References

1. Webb, B. W. and Ma, C. F., 1995, "Single phase liquid impingement heat transfer," *Adv. Heat Transfer*, 26, pp. 105-217.
2. Watson, E. J.,1964, "The radial spread of a liquid jet over a horizontal plane," *J. Fluid Mech.*, 20, pp. 481–499
3. Thomas, S., Hankey, W., Faghri, A., Swanson, T. ,1990, "One-dimensional analysis of the hydrodynamic and thermal characteristics of thin film flows including hydraulic jump and rotation," ASME *J. Heat Transfer* 112:728–735
4. Rahman, M.M., Faghri, A., Hankey, W., 1991, "Computation of turbulent flow in a thin liquid layer of fluid involving a hydraulic jump," *J. Fluids Engr.* 113 pp. 411–418
5. Avedisian, C. T. and Zhao, Z, 2000, "The circular hydraulic jump in low gravity," *Proc. Roy. Soc. London*, 456 pp. 2127-2151
6. Labus, T.L. and DeWitt, K.J., 1978, "Liquid jet impingement normal to a disk in zero gravity," *J. Fluids Engr.* 100, pp. 204–209
7. Miyasaka, Y.,1974, "On the flow of a viscous free boundary jet on a rotating disk," *Bull J. Soc. Mech. Eng.* ,17, pp. 1469–1475
8. Rahman, M.M. and Faghri, A.,1992, "Numerical simulation of fluid flow and heat transfer in a thin liquid film over a rotating disk," *Int. J. Heat Mass Transfer,* 35, pp. 1441–1453
9. Buyevich, Y.A. and Ustinov, V.A., 1994, "Hydrodynamic conditions of transfer processes through a radial jet spreading over a flat surface," *Int. J. Heat Mass Transfer*, 37, pp.165–173
10. Rao, A. and Arakeri, J.H., 1998, "Integral analysis applied to radial film flows," *Int. J. Heat Mass Transfer* , 41, pp. 2757–2767
11. Azuma, T. and Hoshino, T. ,1984, The radial flow of a thin liquid film, 1st–4th Reports. *Bull. J. Soc. Mech. Eng.*, 27, pp. 2739–2770
12. Ozar, B., Cetegen, B. M. and Faghri, A., 2003, "Experiments on the flow of a thin liquid film over a horizontal stationary and rotating disk surface," *Exp. Fluids*, 34, pp. 556-565
13. Chadhury, Z. H., 1964, ''Heat Transfer in a Radial Liquid Jet,'' *J. Fluid Mech.*, 20, pp. 501–511.

14. Wang, X. S., Dagan, Z., and Jiji, L. M., 1989, "Heat Transfer Between a Circular Free Impinging Jet and a Solid Surface with Non-Uniform Wall Temperature of Wall Heat Flux: 1: Solution for the Stagnation Region," *Int. J. Heat Mass Transfer*, 32, pp. 1351–1360.

15. Carper, H. J., and Defenbaugh, D. M., 1978, "Heat Transfer from a Rotating Disk with Liquid Jet Impingement," Proceedings of 6th Int. Heat Transfer Conference, Toronto, pp. 113–118.

16. Carper, Jr., H. J., Saavedra, J. J., and Suwanprateep, T., 1986, "Liquid Jet Impingement Cooling of a Rotating Disk," *ASME J. Heat Transfer*, 108, pp. 540–546.

17. Vader, D. T., Incropera, F. P., and Viskanta, R., 1991, "Local Convective Heat Transfer From a Heated Surface to an Impinging, Planar Jet of Water," *Int. J. Heat Mass Transfer*, 34, pp. 611–623.

18. Stevens, J., and Webb, B. W., 1991, "Local Heat Transfer Coefficients Under and Axisymmetric, Single-Phase Liquid Jet," *ASME J. Heat Transfer*, 113, pp. 71–78.

19. Faghri, A., Thomas, S., and Rahman, M. M., 1993, "Conjugate Heat Transfer from a Heated Disk to a Thin Liquid Film Formed by a Controlled Impinging Jet," *ASME J. Heat Transfer*, 115, pp. 116–123.

20. Aoune, A., and Ramshaw, C., 1999, "Process Intensification: Heat and Mass Transfer Characteristics of Liquid Films on Rotating Discs," *Int. J. Heat Mass Transfer*, 42, pp. 2543–2556.

21. Nusselt WZ (1916) Die Oberflachenkondensation des Wasserdampfes. *Z. Ver Deut. Ing.*, 60, pp. 541–546

22. Ozar, B., Cetegen, B. M., Faghri, A., "Experiments on Heat Transfer in a Thin Liquid Film Flowing Over a Rotating Disk," *ASME J. Heat Transfer*, 126, pp. 184-192

23. Rice, J., Faghri, A., Cetegen, B. M., "Analysis of a free surface film from a controlled liquid impingement jet over a rotating disk including conjugate effects with and without evaporation", Paper No. HT2005-72103, Proc. HT 2005 ASME Summer Heat Transfer Conference, July 17-22, 2005, San Francisco, CA, U.S.A. (also submitted to *Int. J. Heat Mass Transfer)*

APPENDIX A

For determining the thermal entry length for the constant disk surface temperature case, the temperature profile in this region is taken as,

$$\theta = \left[\left(\frac{z}{\delta_T}\right)^2 - 2\left(\frac{z}{\delta_T}\right)\right] \tag{A1}$$

Introducing, $\hat{z} \equiv \frac{\tilde{z}}{\tilde{\delta}_T}$ and $\beta \equiv \frac{\delta_T}{\delta}$, the previously determined velocity profile and the nondimensional temperature profiles become,

$$\tilde{u}_r = 3\frac{\hat{z}}{\tilde{r}\tilde{\delta}_T^{\,2}}\beta^2 \frac{3}{2}\frac{\hat{z}^2}{\tilde{r}\tilde{\delta}_T^{\,3}}\beta^3 \qquad \theta = \hat{z}^2 - 2\hat{z} \tag{A2}$$

substituting into the integral energy equation and integrating to $\hat{z} = 1$, one gets

$$\beta\frac{d}{d\tilde{r}}\left[\frac{\beta^2}{4} - \frac{\beta^3}{20}\right] = \frac{2}{Pe}\left(\frac{r_o}{h_o}\right)^2 \frac{\tilde{r}}{\tilde{\delta}} \tag{A3}$$

since $\beta < 1, \beta^3 << \beta^2$, the equation governing β becomes,

$$\beta^2\frac{d\beta}{d\tilde{r}} = \frac{4}{Pe}\left(\frac{r_0}{h_0}\right)^2 \frac{\tilde{r}}{\tilde{\delta}} \tag{A4}$$

with the condition that $\beta(\tilde{r} = 1) = 0$. The solution is obtained by direct integration as,

$$\beta = \left[\frac{12}{Pe}\left(\frac{r_o}{h_o}\right)^2 \int_1^{\tilde{r}_*} \frac{\tilde{r}d\tilde{r}}{\tilde{\delta}}\right]^{1/3} \tag{A5}$$

If we assume that $\tilde{\delta} \approx 1$, then the integral can be evaluated as,

$$\tilde{r}_* = \left[1 + \frac{Pe}{6}\left(\frac{h_0}{r_0}\right)^2\right]^{1/2} \tag{A6}$$

Since $h_o << r_o$, then, $\tilde{r}_* \approx 1$ or $r_* \approx r_o$. The smallness of the entry region length is utilized in the heat transfer analysis presented in the main body of the paper.

APPENDIX B

Considering the integral momentum equation given by eqn. (9), neglecting the inertial terms on the left hand side allows the direct integration between $\tilde{z}=0$ and $\tilde{z}=\tilde{\delta}$ to yield the velocity profile,

$$\tilde{u}_r = \frac{Re}{Ro}\left(\frac{h_o}{r_o}\right)^2 \tilde{r}\left[\tilde{\delta}\tilde{z} - \frac{\tilde{z}^2}{2}\right] \tag{B1}$$

The corresponding film thickness can be obtained upon integration for the total volumetric flow rate of liquid at any radius leading to the expression for $\tilde{\delta}$ given by eqn. (14). Substitution of this velocity profile into the energy integral equation leads to the following differential equation for a_o,

$$\frac{da_0}{d\tilde{r}} = \frac{1}{\mathrm{Re}\,\mathrm{Pr}}\left(\frac{r_o}{h_o}\right)^2 + \frac{3^{1/3}7}{30}\left(\frac{Ro}{\mathrm{Re}}\right)^{1/3}\left(\frac{r_o}{h_o}\right)^{2/3}\tilde{r}^{-5/3} - \frac{2}{3^{2/3}}\left(\frac{h_o}{r_o}\right)^{1/3}\left(\frac{Ro}{\mathrm{Re}}\right)^{1/3} a_o\tilde{r}^{-8/3} \tag{B2}$$

Since $r_o > h_o$, the last term on the right hand side is small compared to the others. If neglected, eqn. (B2), becomes directly integrable. Applying the condition $a_o(\tilde{r}=1)=1/3$, we get,

$$a_o = \left(\frac{r_o}{h_o}\right)^2 \frac{\tilde{r}-1}{RePr} - \frac{3^{1/3}7}{20}\left(\frac{r_o}{h_o}\right)^{2/3}\left(\frac{Ro}{Re}\right)^{1/3}(\tilde{r}^{-2/3}-1) + \frac{1}{3} \tag{B3}$$

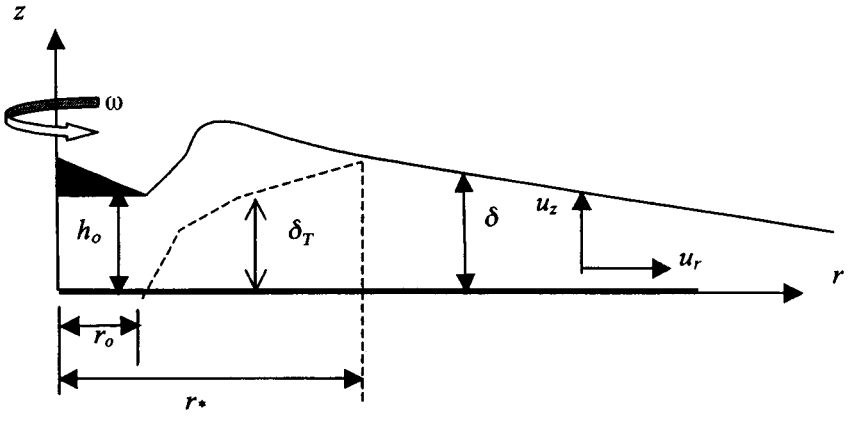

Fig 1: Schematics of the thin film over a rotating disk

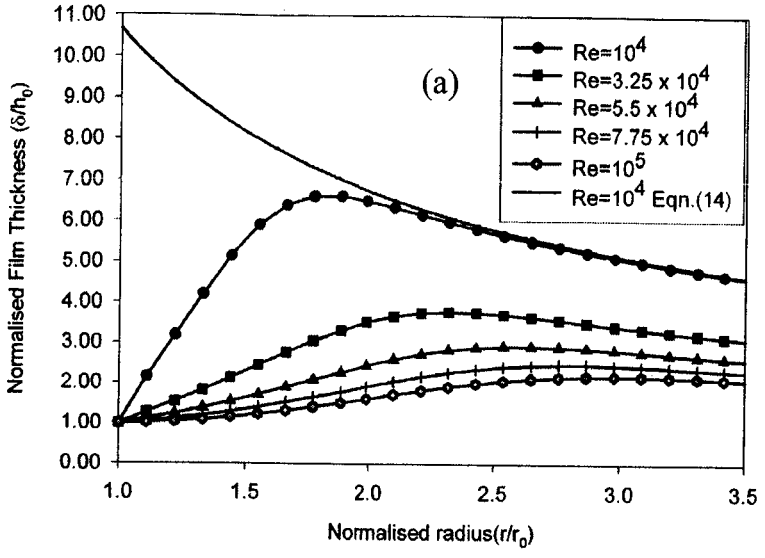

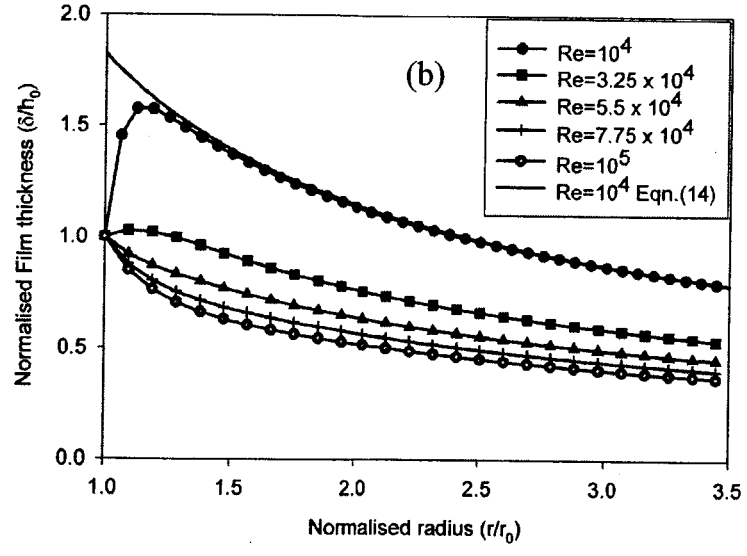

Fig 2: Variation of normalized film thickness as a function of Reynolds number for (a) Ro = 1000 and (b) Ro = 0.5

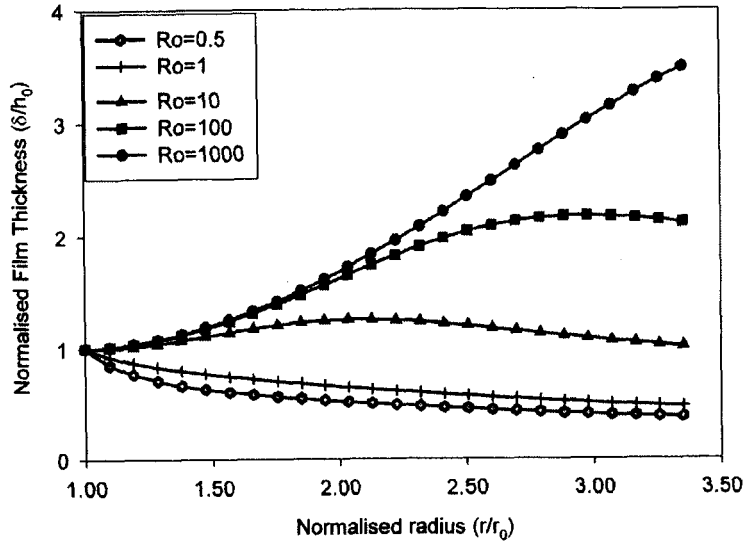

Fig 3: Normalized film thickness variation over the disk surface for different Rossby numbers number for medium flow rate $Re = 10^5$

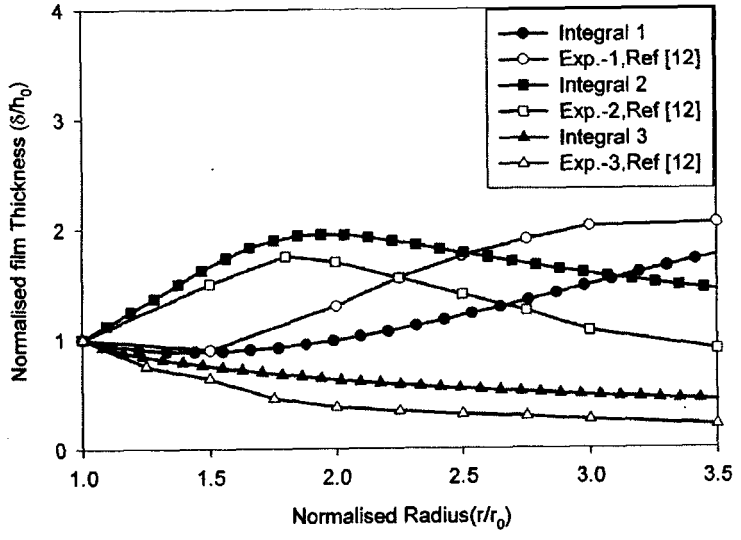

Fig 4: Comparison of film thickness for experimental and theoretical data for several Reynolds number and Rossby numbers. Case 1: $Re = 2.4\ 10^5$, $Ro = 361$; Case 2: $Re = 4.8\ 10^4$, $Ro = 361$; Case 3: $Re = 4.8\ 10^4$, $Ro = 0.4$

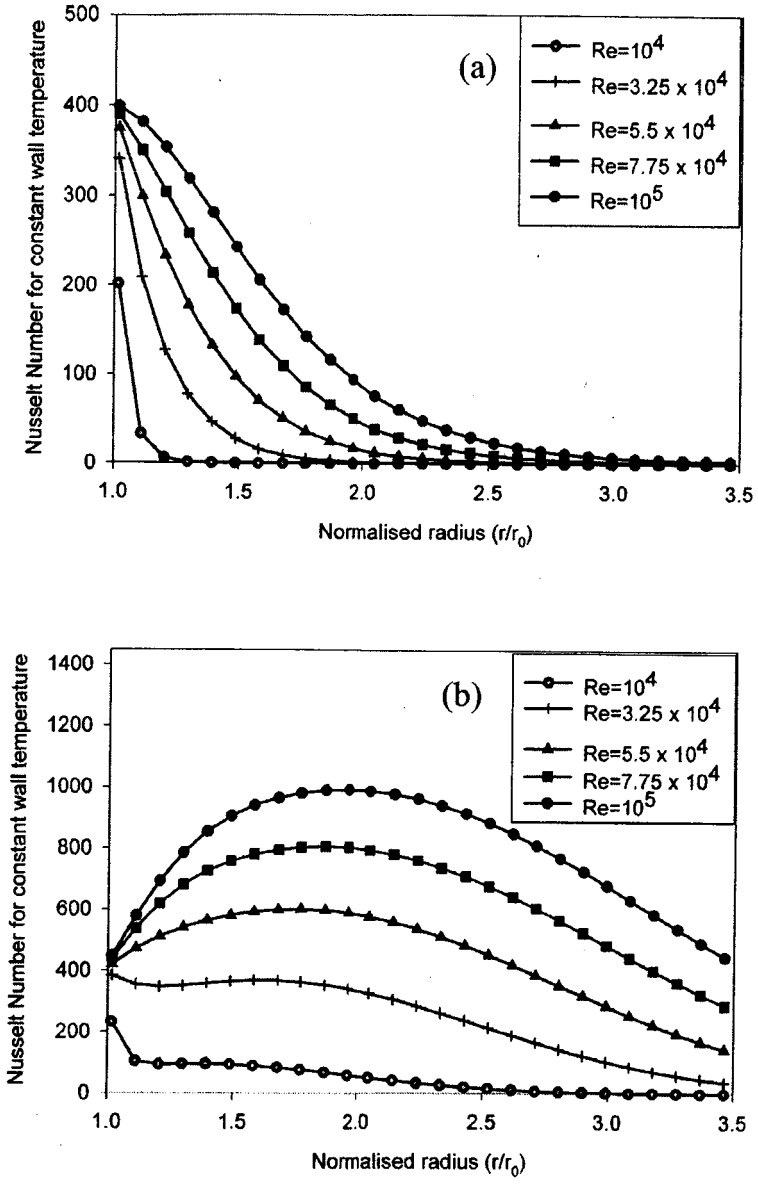

Fig 5: Constant wall temperature Nusselt number variation over the disk surface for different Reynolds numbers for (a) low rotation Ro = 1000 and (b) high rotation Ro = 0.5 cases.

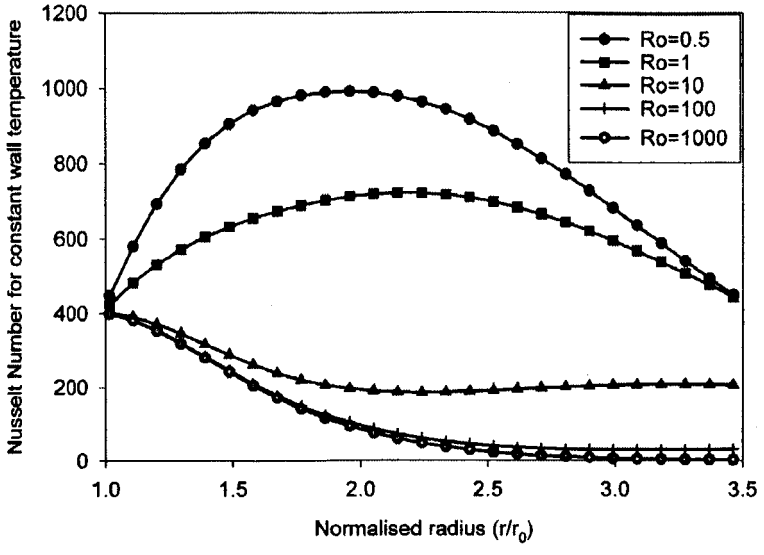

Fig 6: Nusselt number variation for different Rossby numbers for Re = 10^5

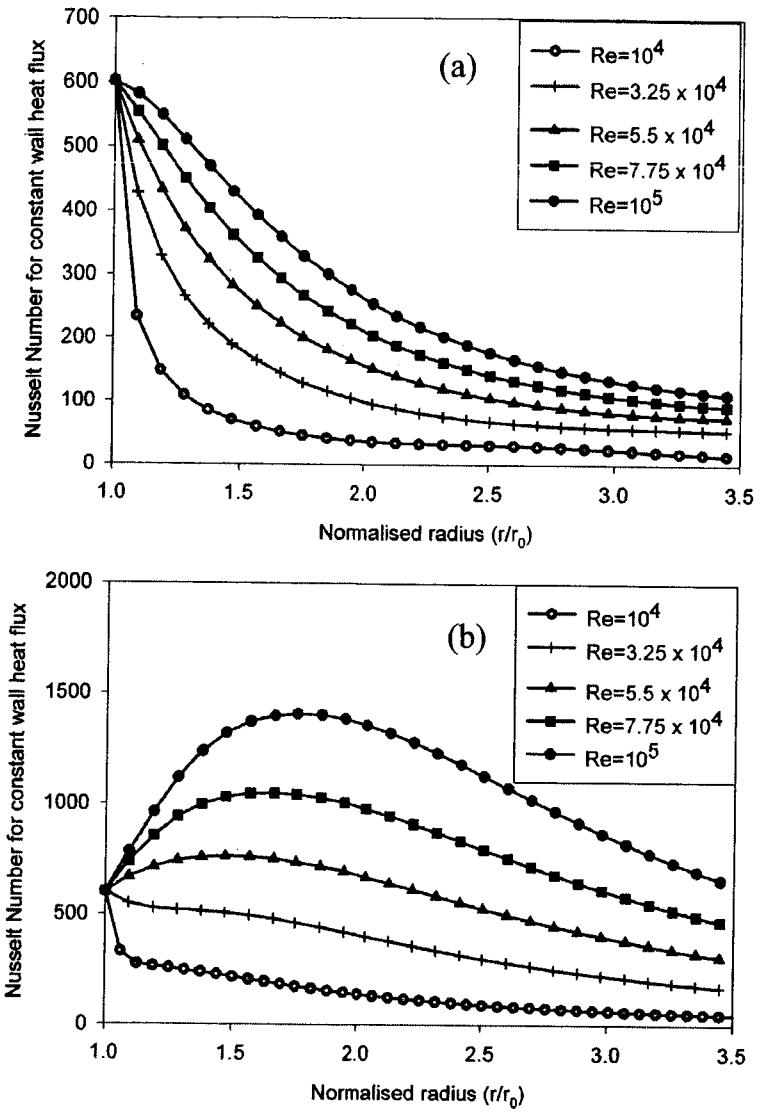

Fig 7: Constant wall heat flux Nusselt number variation over the disk surface for different Reynolds numbers for (a) low rotation Ro = 1000 and (b) high rotation Ro = 0.5 cases.

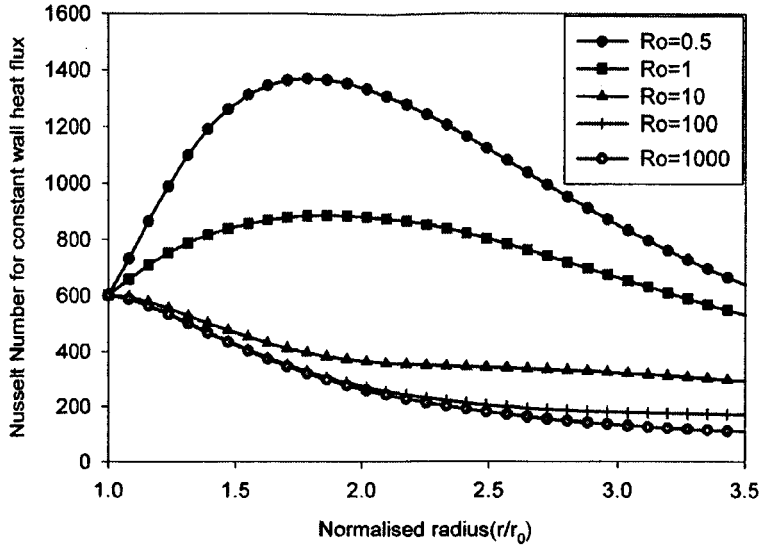

Fig 8: Nusselt number variation for different Rossby numbers for Re = 10^5

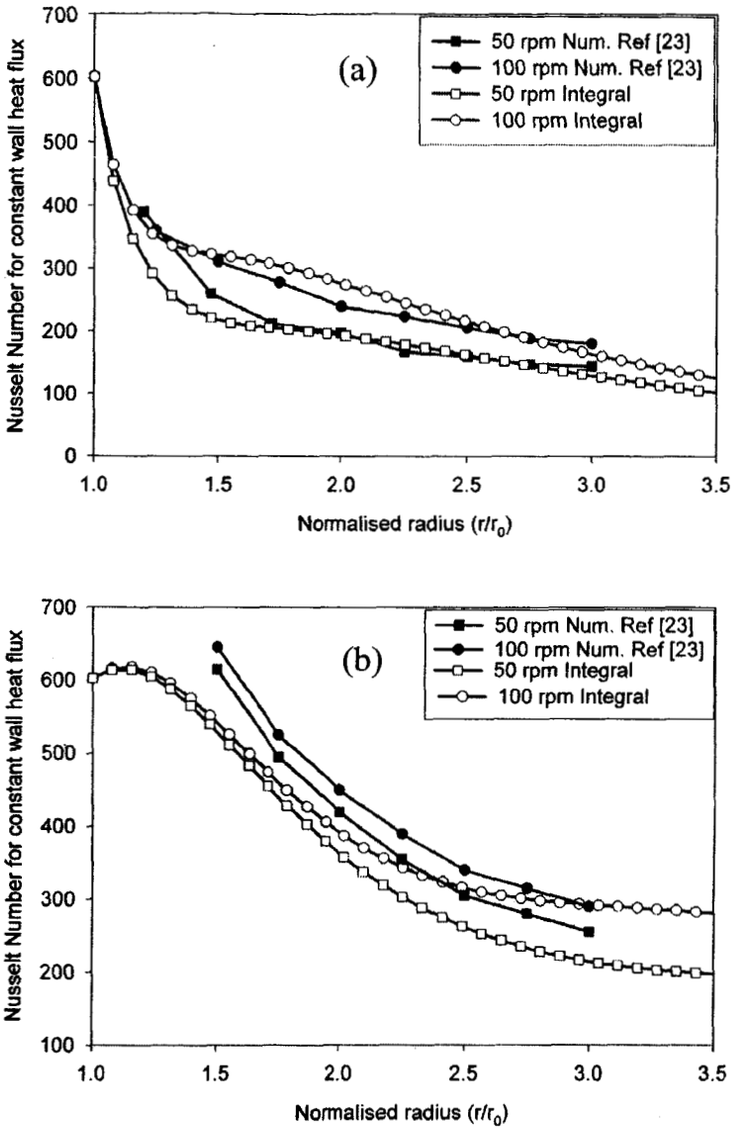

Fig 9: Comparison of calculated Nusselt Number with numerical data of Rice et al [23] for (a) Re = 2.84 10^4 (b) Re = 1.42 10^5 and rotation speeds of 50, 100 rpm

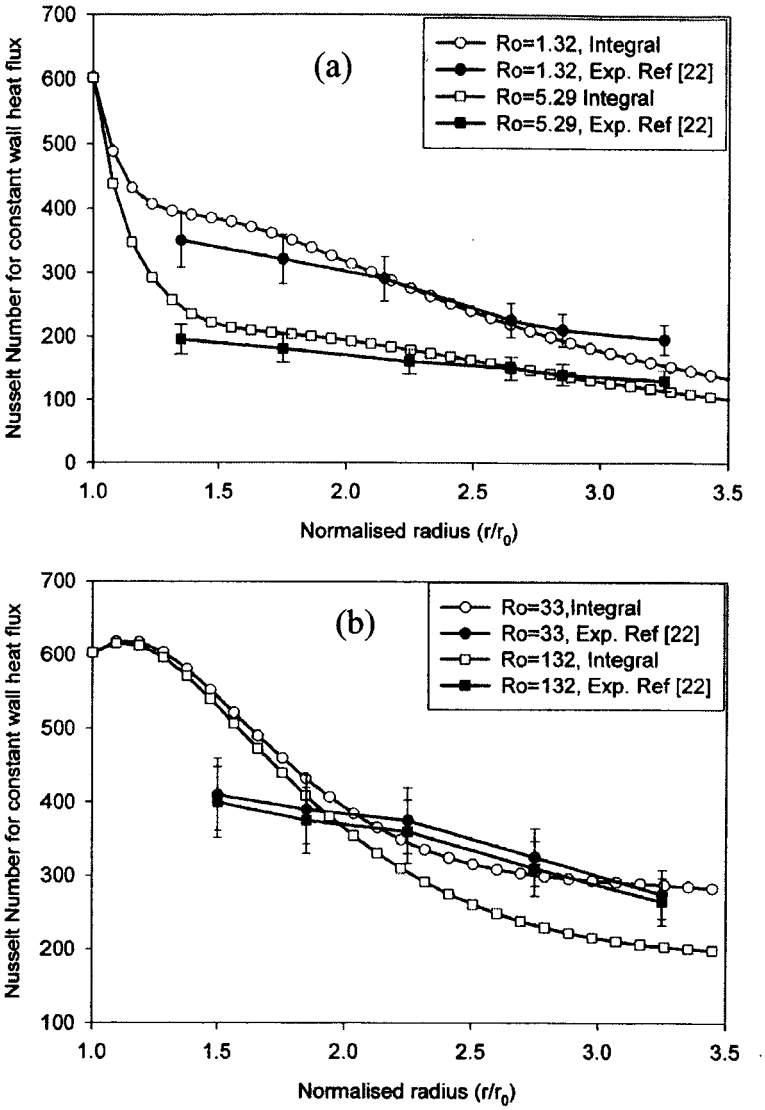

Fig 10: Comparison of Nusselt Number from the integral analysis and the experimental data of Ozar et al [22] for (a) Re=2.85 10^4 and (b) Re=1.42 10^5

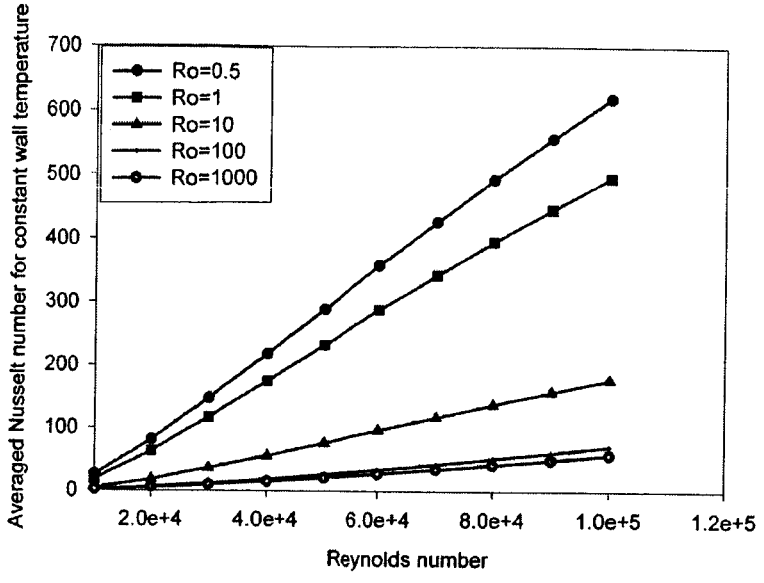

Fig 11: Variation of Average Nusselt Number (based on area) with Reynolds Number for different rotation rates corresponding to the constant wall temperature.

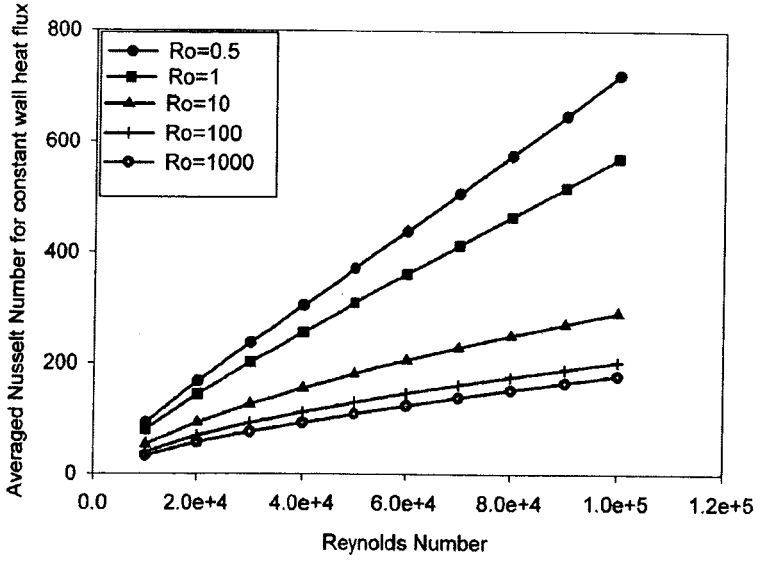

Fig 12: Variation of Average Nusselt Number (based on area) with Reynolds Number for different rotation rates corresponding to the constant wall heat flux case

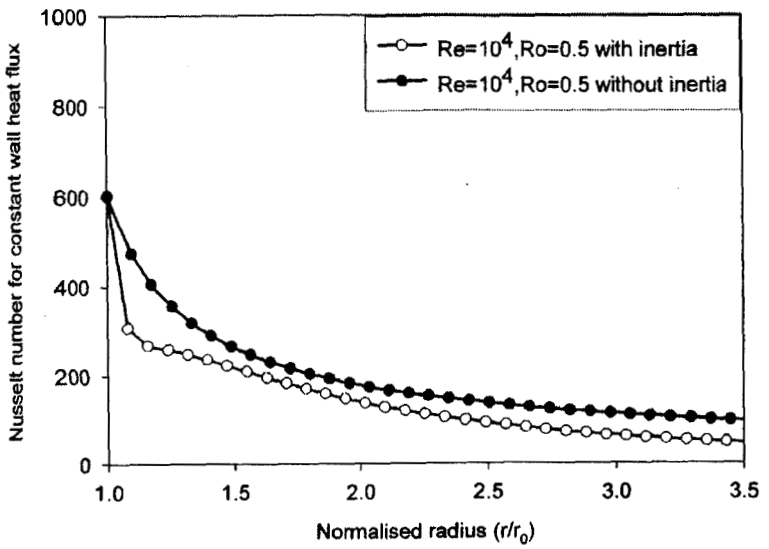

Fig 13: The comparison of the Nusselt number for constant heat flux obtained from full solution and the approximation of negligible inertia